IEC TS 62607-9-1

Edition 1.0 2021-10

TECHNICAL SPECIFICATION

Nanomanufacturing – Key control characteristics – Part 9-1: Traceable spatially resolved nano-scale stray magnetic field measurements – Magnetic force microscopy

IEC TS 62607-9-1:2021-10(en)

IEC Central Office
3, rue de Varembé
CH-1211 Geneva 20
Switzerland

Tel.: +41 22 919 02 11
info@iec.ch
www.iec.ch

About the IEC
The International Electrotechnical Commission (IEC) is the leading global organization that prepares and publishes International Standards for all electrical, electronic and related technologies.

About IEC publications
The technical content of IEC publications is kept under constant review by the IEC. Please make sure that you have the latest edition, a corrigendum or an amendment might have been published.

IEC publications search - webstore.iec.ch/advsearchform
The advanced search enables to find IEC publications by a variety of criteria (reference number, text, technical committee, …). It also gives information on projects, replaced and withdrawn publications.

IEC Just Published - webstore.iec.ch/justpublished
Stay up to date on all new IEC publications. Just Published details all new publications released. Available online and once a month by email.

IEC Customer Service Centre - webstore.iec.ch/csc
If you wish to give us your feedback on this publication or need further assistance, please contact the Customer Service Centre: sales@iec.ch.

IEC online collection - oc.iec.ch
Discover our powerful search engine and read freely all the publications previews. With a subscription you will always have access to up to date content tailored to your needs.

Electropedia - www.electropedia.org
The world's leading online dictionary on electrotechnology, containing more than 22 000 terminological entries in English and French, with equivalent terms in 18 additional languages. Also known as the International Electrotechnical Vocabulary (IEV) online.

IEC TS 62607-9-1

Edition 1.0 2021-10

TECHNICAL SPECIFICATION

colour inside

Nanomanufacturing – Key control characteristics – Part 9-1: Traceable spatially resolved nano-scale stray magnetic field measurements – Magnetic force microscopy

INTERNATIONAL ELECTROTECHNICAL COMMISSION

ICS 07.120

ISBN 978-2-8322-1032-9

CONTENTS

INTERNATIONAL ELECTROTECHNICAL COMMISSION

_____

NANOMANUFACTURING – KEY CONTROL CHARACTERISTICS –

Part 9-1: Traceable spatially resolved nano-scale stray magnetic field measurements – Magnetic force microscopy

FOREWORD

1) The International Electrotechnical Commission (IEC) is a worldwide organization for standardization comprising all national electrotechnical committees (IEC National Committees). The object of IEC is to promote international co-operation on all questions concerning standardization in the electrical and electronic fields. To this end and in addition to other activities, IEC publishes International Standards, Technical Specifications, Technical Reports, Publicly Available Specifications (PAS) and Guides (hereafter referred to as "IEC Publication(s)"). Their preparation is entrusted to technical committees; any IEC National Committee interested in the subject dealt with may participate in this preparatory work. International, governmental and non-governmental organizations liaising with the IEC also participate in this preparation. IEC collaborates closely with the International Organization for Standardization (ISO) in accordance with conditions determined by agreement between the two organizations.
2) The formal decisions or agreements of IEC on technical matters express, as nearly as possible, an international consensus of opinion on the relevant subjects since each technical committee has representation from all interested IEC National Committees.
3) IEC Publications have the form of recommendations for international use and are accepted by IEC National Committees in that sense. While all reasonable efforts are made to ensure that the technical content of IEC Publications is accurate, IEC cannot be held responsible for the way in which they are used or for any misinterpretation by any end user.
4) In order to promote international uniformity, IEC National Committees undertake to apply IEC Publications transparently to the maximum extent possible in their national and regional publications. Any divergence between any IEC Publication and the corresponding national or regional publication shall be clearly indicated in the latter.
5) IEC itself does not provide any attestation of conformity. Independent certification bodies provide conformity assessment services and, in some areas, access to IEC marks of conformity. IEC is not responsible for any services carried out by independent certification bodies.
6) All users should ensure that they have the latest edition of this publication.
7) No liability shall attach to IEC or its directors, employees, servants or agents including individual experts and members of its technical committees and IEC National Committees for any personal injury, property damage or other damage of any nature whatsoever, whether direct or indirect, or for costs (including legal fees) and expenses arising out of the publication, use of, or reliance upon, this IEC Publication or any other IEC Publications.
8) Attention is drawn to the Normative references cited in this publication. Use of the referenced publications is indispensable for the correct application of this publication.
9) Attention is drawn to the possibility that some of the elements of this IEC Publication may be the subject of patent rights. IEC shall not be held responsible for identifying any or all such patent rights.

IEC TS 62607-9-1 has been prepared by IEC technical committee 113: Nanotechnology for electrotechnical products and systems. It is a Technical Specification.

The text of this Technical Specification is based on the following documents:

Draft	Report on voting
113/584/DTS	113/606/RVDTS

Full information on the voting for its approval can be found in the report on voting indicated in the above table.

The language used for the development of this Technical Specification is English.

This document was drafted in accordance with ISO/IEC Directives, Part 2, and developed in accordance with ISO/IEC Directives, Part 1 and ISO/IEC Directives, IEC Supplement, available at www.iec.ch/members_experts/refdocs. The main document types developed by IEC are described in greater detail at www.iec.ch/standardsdev/publications.

A list of all parts of the IEC TS 62607 series, published under the general title *Nanomanufacturing – Key control characteristics*, can be found on the IEC website.

The committee has decided that the contents of this document will remain unchanged until the stability date indicated on the IEC website under webstore.iec.ch in the data related to the specific document. At this date, the document will be

- reconfirmed,
- withdrawn,
- replaced by a revised edition, or
- amended.

IMPORTANT – The "colour inside" logo on the cover page of this document indicates that it contains colours which are considered to be useful for the correct understanding of its contents. Users should therefore print this document using a colour printer.

INTRODUCTION

Measurements of magnetic fields that are homogeneous over macroscopic volumes can be made traceable to the SI standards, and traceable calibration chains from the national metrology institutes to the end users are well-established.

However, many important industrial applications such as magneto-resistive position, angle, or motion control rely on precision sensing of spatially varying magnetic fields. Such spatially varying magnetic fields can, for example, be generated by a magnetic bit pattern of a magnetic encoder scale. Today, magnetic encoder bit patterns have typically a lateral periodicity above 100 µm. Based on stray field interpolation, such encoders are applied, for example, for precision positioning systems with sub-micrometre resolution. However, such precision positioning requires reliable local field measurements which are not yet underpinned by any suitable standards.

Today, local magnetic stray field measurements with resolutions from above 50 µm down to below 500 nm can be realized by scanning magnetic field detection (SMF) methods with different field sensors such as Hall sensors, magneto-resistive (MR) sensors and magnetically coated tips on an oscillating cantilever (magnetic force microscopy (MFM)), or with imaging techniques like Kerr and magneto-optical indicator film (MOIF) microscopy. Achievable spatial resolution and typical scanning area are compared in Figure 1.

MFM provides a significantly higher resolution than other SMF techniques and MOIF (see Figure 1) and can therefore be considered as the standard tool for nano-scale investigations of the local magnetic properties of magnetic nanostructures, thin films and devices [1][1]. However, despite its wide use, MFM measurements per se only deliver purely qualitative stray field images that cannot be applied for quantitative data analysis. This results from the fact that the measured signal strongly depends on the properties of the magnetic tip, the mechanical properties of the cantilever and the sensitivity of the detection device. Hence a calibration that includes the characterization of the magnetic tip and the microscope is needed if the MFM method is to be used to provide values of key control characteristics (KCCs) which are ultimately traceable to national calibration standards.

This document aims to provide industry end users, instrument manufactures and calibration laboratories with a description of traceable calibration procedures based on reference materials with well-defined local stray field distributions. This document includes the description of suitable reference samples, the evaluation of MFM key parameters required for the method, and the determination of the instrument calibration function (ICF). Due to the finite dimension of the tip, a spatial broadening of the MFM signal is unavoidable. Mathematically this broadening can be described by the convolution of the ICF and the real magnetic field structure of the sample to be measured. Vice versa, a quantitative analysis of the measured data is achieved by a deconvolution of the MFM measurement data using the ICF. The description of this process is the key part of this document.

1 Numbers in square brackets refer to the Bibliography.

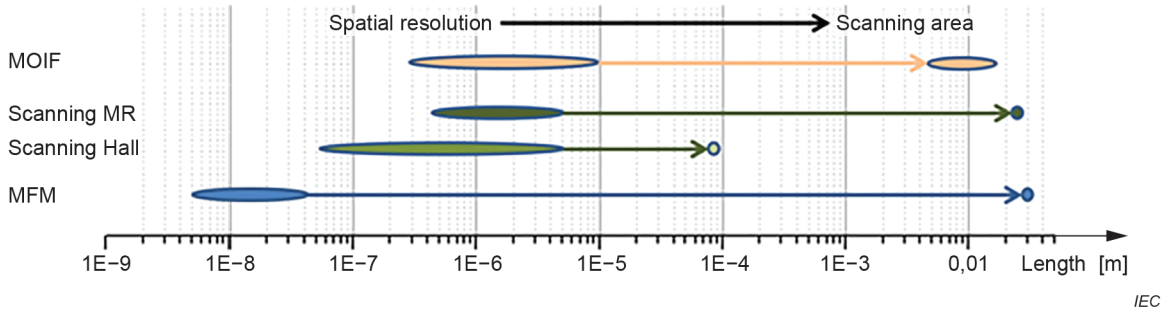

Figure 1 – Spatial resolution of magnetic stray field characterization techniques and their possible maximum scan area

The MFM technique as described in this document has a resolution down to about 10 nm to 20 nm (depending on the signal-to-noise ratio of the instrument), which is at least one order of magnitude superior to other common characterization techniques for spatially varying magnetic fields. MFM systems operated at ambient conditions typically can achieve a resolution of around 50 nm [1]. With optimized tips, a resolution down to below 20 nm is possible [2]. The highest resolution in MFM is achieved in vacuum. With very precise tip–sample distance control [3] and high-resolution tips [4], a resolution down to 10 nm could be demonstrated.

While the MFM technique has the best precision and accuracy of the test methods (see Figure 1), as a scanning technique it is comparatively slow, requires specific ambient conditions such as stable temperatures and can only be used for samples which are flat and smooth on a micrometre scale (depending on the scanning unit). For routine statistical process control (SPC) of the manufacturing process, it may not be suitable in many use cases. Therefore, it is anticipated that the MFM technique needs to be complemented, for example, by:

- the magneto-optical indicator film technique (MOIF), which, as an imaging process, allows high throughput;
- scanning Hall or MR test methods, which can easily be calibrated in homogeneous external fields. In CMOS technique, arrays of parallel Hall sensors can be prepared and thus a high throughput can be achieved in a scanning process.

Wherever possible, existing relevant scanning probe microscopy (SPM) standards are referred to, especially those developed by ISO/TC 201 like ISO 18115-2 [5] and ISO 11952 [6].

In summary, this document provides a traceable method for nanometre-resolution measurements of magnetic field patterns, which is the basis for precise control of fabrication processes and final product qualification. The key control characteristics for those products are very product specific (see, for example, IEC TS 62622:2012 [7]).

NANOMANUFACTURING – KEY CONTROL CHARACTERISTICS –

Part 9-1: Traceable spatially resolved nano-scale stray magnetic field measurements – Magnetic force microscopy

1 Scope

This part of IEC 62607 establishes a standardized method to characterize spatially varying magnetic fields with a spatial resolution down to 10 nm for flat magnetic specimens by magnetic force microscopy (MFM). MFM primarily detects the stray field component perpendicular to the sample surface. The resolution is achieved by the calibration of the MFM tip using magnetically nanostructured reference materials.

The objective of this document is to define and describe:

- reference materials for traceable high resolution magnetic stray field measurements;
- the calibration procedures to determine the instrument calibration function (ICF) and, if required, MFM key parameters entering the deconvolution process;
- the deconvolution process which allows to calculate quantitative stray field data from the measured MFM data using the ICF;
- the evaluation of the measurement uncertainty, including the prevention of potential artefacts which can occur during the measurement leading to a misinterpretation of the results.

2 Normative references

There are no normative references in this document.

3 Terms and definitions

For the purposes of this document, the following terms and definitions apply.

ISO and IEC maintain terminological databases for use in standardization at the following addresses:

- IEC Electropedia: available at http://www.electropedia.org/
- ISO Online browsing platform: available at http://www.iso.org/obp

3.1 General terms

3.1.1
key control characteristic
KCC
key performance indicator
measurement process characteristic which can affect compliance with regulations and quality, reliability or subsequent application of the measurement result

Note 1 to entry: The measurement of a key control characteristic is described in a standardized measurement procedure with known accuracy and precision.

Note 2 to entry: It is possible to define more than one measurement method for a key control characteristic, if the correlation of the results is well-defined and known.

Note 3 to entry: In IATF 16949 [8] the term "special characteristic" is used for a KCC. The term key control characteristic is preferred since it signals directly the relevance of the parameter for the quality of the final product.

3.2 General terms related to magnetic stray field characterization

3.2.1
magnetic-force microscopy
MFM
atomic force microscopy mode employing a probe assembly that monitors both atomic forces and magnetic interactions between the probe tip and a surface

[SOURCE: ISO 18115-2:2013, 3.15]

3.2.2
magneto-optical indicator film technique
MOIF technique
method of mapping the magnetic field above a sample surface by a thin magneto-optical indicator film

Note 1 to entry: The magnetic fields induce a perpendicular magnetization component in the active layer of the detector, which is recorded with the Faraday effect.

3.2.3
dynamic mode scanning force microscopy
scanning magnetic force microscopy mode in which the relative positions of the probe tip and sample vary in a sinusoidal manner in time at each point in the image

Note 1 to entry: The sinusoidal oscillation is usually in the form of a vibration in the z-direction and is often driven at a frequency close to, and sometimes equal to, the cantilever resonance frequency.

Note 2 to entry: The signal measured can be the amplitude, the phase shift, or the resonance frequency shift of the cantilever.

[SOURCE: ISO 18115-2:2013, 3.6, modified – The source uses the term "dynamic-mode AFM" instead of "dynamic mode scanning force microscopy" and the term "AFM mode" instead of "scanning magnetic force microscopy mode"]

3.2.4
intermittent contact mode
mode of scanning the probe where the probe is operated with a sinusoidal z-displacement modulation such that the probe tip makes contact with the sample for a fraction of the sinusoidal cycle

[SOURCE: ISO 18115-2:2013, 5.73]

3.2.5
non-contact magnetic-force microscopy
NC-MFM
dynamic mode scanning force microscopy (3.2.3) in which the probe tip is operated at such a distance from the surface that it samples the weak attractive van der Waals or other forces

3.2.6
scanning magnetic field microscopy
SMF microscopy
method of measuring and mapping the magnetic field from a sample surface by mechanically scanning a probe above the sample surface

Note 1 to entry: This generic term encompasses *scanning Hall probe magnetometry* (3.2.7) and *scanning MR magnetometry* (3.2.8).

3.2.7
scanning Hall probe magnetometry
SHM
scanning magnetic field microscopy (3.2.6) mode in which a Hall probe is used as the scanning sensor to measure and map the magnetic field from a sample surface by acquiring a Hall voltage

[SOURCE: ISO 18115-2:2013, 3.23, modified – The phrase "scanning magnetic field microscopy" is used instead of "SPM" and the phrase "by acquiring a Hall voltage" is added]

3.2.8
scanning MR magnetometry
SMR magnetometry
scanning magnetic field microscopy (3.2.6) mode in which a magneto-resistive sensor probe on a cantilever is scanned over a magnetic sample surface to measure the *magnetic field distribution* (3.3.1) by acquiring a magneto-resistive voltage

[SOURCE: ISO 18115-2:2013, 3.25, modified – The "phrase "scanning magnetic field microscopy" is used instead of "SPM" and the phrase "magnetic field distribution" is used instead of "two-dimensional magnetic images"]

3.3 Terms related to the measurement method described in this document

3.3.1
magnetic field distribution
spatially resolved magnetic field data array in the x-y-plane with the x-, y-direction in the sample plane and the z-direction along the sample surface normal with a spatial resolution dx, dy at a distance d above the surface of a test specimen

3.3.2
raw data distribution
spatially resolved MFM raw data array with the x-, y-direction in the sample plane and the z-direction along the sample surface normal at a distance d above the surface of a test specimen

3.3.3
magnetic force
force acting between magnetic volumes

Note 1 to entry: In SPM, the magnetic dipoles are usually incorporated as ferromagnetic material in the probe tip and it is the magnetic field of the sample that is measured.

[SOURCE: ISO 18115-2:2013, 5.8, modified – The phrase "magnetic volumes" is used instead of "magnetic dipoles in a magnetic field"]

3.3.4
magnetically coated probe tip
probe which is coated with a thin magnetic layer on the tip side of the cantilever

Note 1 to entry: The magnetic layer creates a magnetic volume that interacts with the sample magnetic field and thus probes it.

3.3.5
constant height mode
mode of scanning the probe tip over the sample surface at a constant height of the centre of the oscillation of the tip apex relative to the surface plane of the sample during the scan

[SOURCE: ISO 18115-2:2013, 5.34, modified –"over the surface" is replaced with "of the centre of the oscillation of the tip apex relative to the surface plane of the sample".]

3.3.6
measurement height
value of the constant height of the centre of the oscillation of the tip apex relative to the surface plane of the sample during a measurement in *constant height mode* (3.3.5)

3.3.7
measurement plane
plane at constant height above the surface where the raw data distribution is measured in *constant height mode* (3.3.5)

3.3.8
cantilever oscillation
sinusoidal z-displacement of the cantilever and thus the tip in *dynamic mode scanning force microscopy* (3.2.3)

Note 1 to entry: The z-displacement is typically induced by the oscillation of the cantilever by means of an excitation piezo, the driven frequency is close to the cantilever resonance frequency.

3.3.9
cantilever
thin force-sensing support for a *magnetically coated probe tip* (3.3.4) joined to the *cantilever chip* (3.3.10) at the end furthest from the probe tip

[SOURCE: ISO 18115-2:2013, 5.18, modified – The phrase "a magnetically coated probe tip" is used instead of "a probe tip".]

3.3.10
cantilever chip
small piece, usually of silicon, on which the *cantilever* (3.3.9) with the *magnetically coated probe tip* (3.3.4) has been fabricated and to which it is still attached as a convenient supporting structure in the probe assembly (3.3.12)

[SOURCE: ISO 18115-2, 5.26, modified – The phrase "with the magnetically coated probe tip" is added.]

3.3.11
chip holder
structure on which the *cantilever chip* (3.3.10) with the *cantilever* (3.3.9) and the *magnetically coated probe tip* (3.3.4) are mounted

Note 1 to entry: The chip holder, chip, cantilever, and probe comprise the *probe assembly* (3.3.12).

[SOURCE: ISO 18115-2:2013, 5.27, modified – The phrase "the magnetically coated" is added.]

3.3.12
probe assembly
structure comprising the *chip holder* (3.3.11), *cantilever chip* (3.3.10), *cantilever* (3.3.9) and *magnetically coated probe tip* (3.3.4) including a provision to drive a sinusoidal oscillation of the cantilever in the form of a vibration in the z-direction

Note 1 to entry: This provision typically is an excitation piezo, see ISO 18115-2.

[SOURCE: ISO 18115-2:2013, 5.20, modified– The phrase "magnetically coated probe tip" is used instead of "probe" and the phrase "including a provision to drive a sinusoidal oscillation of the cantilever in the form of a vibration in the z-direction" is added.]

3.3.13
excitation piezo
provision to drive a sinusoidal oscillation of the *cantilever* (3.3.9) in the form of a vibration in the z-direction exploiting the variation of a piezo active material induced by a sinusoidal electric drive signal

Note 1 to entry: See ISO 18115-2.

3.3.14
MFM observation variable
phase shift between sinusoidal cantilever drive signal and cantilever oscillation at fixed excitation frequency and excitation amplitude

Note 1 to entry: In principle, other measurands can also be exploited to detect the interaction between magnetic tip and sample stray field, e.g. the frequency shift of the resonance frequency of the oscillating cantilever.

3.3.15
phase shift signal
$\Delta\varphi$
MFM observation variable (3.3.14) defined as the phase shift between sinusoidal cantilever drive signal and cantilever oscillation at fixed excitation frequency and excitation amplitude

Note 1 to entry: The signal may be corrected by a constant offset.

3.3.16
signal detector
detector that transforms the amplitude and temporal course of the cantilever oscillation into an electrical signal

Note 1 to entry: In this case a light pointer combined with a sensitive photo detector (PSD).

3.3.17
signal analysis system
system to extract and record the *MFM observation variable* (3.3.14) as a function of the lateral displacement of the tip

Note 1 to entry: In this case a system to extract the phase shift between the cantilever driving sinusoidal oscillation and the signal detected by the signal detector. The phase shift may be offset corrected.

3.3.18
z-scanner
element for the realization of the vertical displacement of the specimen/probe distance during x-y-scanning

Note 1 to entry: See ISO 18115-2:2013, 5.136.

3.3.19
x-y-scanner
element for realization of the lateral displacement of the probe or of the specimen in the x-y-plane

3.3.20
data pre-processing
raw data treatment to remove known artefacts of the measurement process

3.3.21
data levelling
form of *data pre-processing* (3.3.20) to eliminate unwanted features from scan lines, such as drift and offsets

3.3.22
magnetic field reference sample
magnetic sample whose *magnetic field distribution* (3.3.1) above the sample surface is well-known or can be calculated

3.3.23
cantilever resonance quality factor
Q
energy stored in a cantilever for a particular resonance peak divided by the average energy lost per radian of oscillation, this average being over one cycle

Note 1 to entry: A practical method of measuring the cantilever resonance quality factor is to record a resonance curve as a function of frequency. Q is approximately equal to the resonance frequency divided by the bandwidth of the resonance, and this approximation is excellent for quality factors above about 4.

Note 2 to entry: The bandwidth of the resonance can be measured from a plot of the square of the amplitude against frequency. The bandwidth is the frequency interval between the two points 3 dB below the peak maximum on either side of the peak. This is, to an error of less than 0,25 %, the full width at half maximum height (FWHM) of this curve, so the FWHM can be judged a more convenient and sufficiently accurate measure of bandwidth for many practical purposes.

[SOURCE: ISO 18115-2:2013, 5.127, modified – The term is "cantilever resonance quality factor" instead of merely "quality factor" and, accordingly, the more general phrase "a given resonator" is replaced with "a cantilever". The original Note 1 is omitted.]

3.3.24
oscillation amplitude
A_{osc}
tip oscillation amplitude caused by the *cantilever oscillation* (3.3.8) in *dynamic mode scanning force microscopy* (3.2.3)

Note 1 to entry: The oscillation amplitude for an approached intermittent contact mode measurement and for a constant height measurement may be different.

3.3.25
lift height
z^{lh}
vertical distance by which the distance of the oscillation centre of the probe's tip apex to the sample surface is increased in between intermittent contact mode and constant height measurements

3.3.26
measurement height
z
distance of the oscillation centre of the probe's tip apex to the sample surface in a dynamic mode MFM

Note 1 to entry: Instruments typically give a *lift height* (3.3.25) value for the MFM measurement in a dynamic mode. The tip–sample distance is the sum of the lift height and the *oscillation amplitude* (3.3.24) as measured when the probe is approached to the sample surface.

3.3.27
scan size
Sx, Sy
length and width of the scanned area in the scan plane

3.3.28
pixel size
Δx, Δy
length and width of the area represented by each measured point in a 2D raster image

3.3.29
cantilever canting angles
θ, φ
azimuthal and polar angles describing the tilt of the cantilever with respect to the MFM measurement plane in polar coordinates

Note 1 to entry: See ISO 18115-2:2013, 5.92 Note 2 to entry and 5.119.

3.3.30
tip magnetization orientation
M_{tip}
sign of the net effective magnetic charge distribution of the magnetic tip, described as "up" or "down" or as "+" or "−"

Note 1 to entry: The underlying tip magnetization distribution depends on the structure of the probe tip and the coating method of the magnetic thin layer.

Note 2 to entry: The tip can be magnetized in a magnetic field higher than the tip coercive field normal to the cantilever.

3.3.31
effective magnetic charge distribution
σ^{eff}
hypothetical 2D magnetic monopole distribution that results in the same magnetic field above a sample or below a magnetically coated tip as the underlying 3D magnetic volume material

3.3.32
sample under test
SUT
material whose magnetic field distribution is to be measured

3.3.33
spring constant
force constant
C
quotient of the applied normal force at the probe tip by the deflection of the cantilever in that direction at the probe tip position

[SOURCE: ISO 18115-2:2013, 5.92]

3.3.34
pseudo-Wiener deconvolution
deconvolution applying a pseudo-Wiener-filter for noise suppression in a deconvolution in Fourier space with regularization parameter α

Note 1 to entry: The formula that applies is as follows, where the asterisk marks the complex conjugate:

$$A(\boldsymbol{k},z)=\frac{B(\boldsymbol{k},z)}{C(\boldsymbol{k},z)} \quad \rightarrow \quad A(\boldsymbol{k},z)=B(\boldsymbol{k},z)\frac{C^{*}(\boldsymbol{k},z)}{\left|C(\boldsymbol{k},z)\right|^{2}+\alpha}$$

3.3.35
regularization parameter
α
constant in the *pseudo-Wiener deconvolution* (3.3.34) that approximates the noise characteristics of the image

3.3.36
tip transfer function
TTF
F^{TTF}
distribution of the stray field gradient generated by the magnetically coated tip in the measurement plane

3.3.37
discrimination
data treatment process where the data entries in a data distribution are dichotomized resulting in a binary data set with entries +1 or −1

Note 1 to entry: The dichotomization is effected on the basis of a threshold value t as discrimination criterion. Data entries less than t are assigned the value −1, data entries greater than or equal to t are assigned the value +1.

3.4 Key control characteristics measured according to this document

3.4.1
magnetic field distribution of the reference sample
H_z^{ref}
magnetic field distribution (3.3.1) of the perpendicular magnetic field component of the reference sample in the *measurement plane* (3.3.7)

3.4.2
measured phase shift distribution of the reference sample
$\Delta\varphi^{\mathrm{ref}}$
raw data distribution (3.3.2) being the *phase shift signal* (3.3.15) distribution in *dynamic mode scanning force microscopy* (3.2.3) of the reference sample measured in the *measurement plane* (3.3.7) in *constant height mode* (3.3.5)

3.4.3
instrument calibration function
ICF
scanning magnetic field microscopy (3.2.6) system response function in real or partial Fourier space that relates the measured signal to the magnetic field distribution

Note 1 to entry: In this case, it relates the *measured phase shift distribution of the sample under test* (3.4.4) to the underlying *magnetic field distribution of the sample under test* (3.4.5). For magnetic force microscopy, the ICF is a linear function of the frequency spectrum of the measured signal. The ICF is calibrated using a reference sample.

3.4.4
measured phase shift distribution of the sample under test
$\Delta\varphi^{\mathrm{SUT}}$
measured *phase shift signal* (3.3.15) distribution with respect to the perpendicular magnetic field component of the sample under test in the *measurement plane* (3.3.7)

3.4.5
magnetic field distribution of the sample under test
H_z^{SUT}
magnetic field distribution (3.3.1) of the perpendicular magnetic field component of the sample under test in the *measurement plane* (3.3.7)

Note 1 to entry: The magnetic field *raw data distribution* (3.3.2) being the *phase shift signal* (3.3.15) distribution in a *dynamic mode scanning force microscopy* (3.2.3) of the sample under test measured in the *measurement plane* (3.3.7) in *constant height mode* (3.3.5).

3.5 Symbols and abbreviated terms

Abbreviation	Description
DFT	discrete Fourier transform
ICF	instrument calibration function
KCC	key control characteristic
MFM	magnetic force microscopy
MOIF	magneto-optical indicator film
MR	magneto-resistive
NC-MFM	non-contact magnetic-force microscopy
SHM	scanning Hall microscopy
SMF	scanning magnetic field
SUT	sample under test
TTF	tip transfer function

Symbol	Corresponding uncertainty (if applicable)	Description
α	$u\alpha$	regularization parameter
A_{osc}	uA_{osc}	tip oscillation amplitude
C	uC	cantilever spring constant
δ_{DW}	$u\delta_{\mathrm{DW}}$	domain wall transition width
D		instrument sensitivity
$f(x,y)$	$uf(x,y)$	domain wall kernel
$\Delta\varphi^{\mathrm{ref}}(x,y,z)$ / $\Delta\varphi^{\mathrm{ref}}(\boldsymbol{k},z)$	$u\Delta\varphi^{\mathrm{ref}}$	reference sample measurement raw data (phase shift data) in real / partial Fourier space
$\Delta\varphi^{\mathrm{SUT}}(x,y,z)$ / $\Delta\varphi^{\mathrm{SUT}}(\boldsymbol{k},z)$	$u\Delta\varphi^{\mathrm{rSUT}}$	SUT measurement raw data (phase shift data) in real / partial Fourier space
$\Delta A = \Delta x \times \Delta y$	$u\Delta A$, $u\Delta x$, $u\Delta y$	pixel size in x- / y-direction
H		environmental humidity
$H_z^{\mathrm{ref}}(x,y,z)$ / $H_z^{\mathrm{ref}}(\boldsymbol{k},z)$	uH_z^{ref}	z-component of the magnetic field distribution of the reference sample in real / partial Fourier space
$H_z^{\mathrm{SUT}}(x,y,z)$ / $H_z^{\mathrm{SUT}}(\boldsymbol{k},z)$	uH_z^{SU}	z-component of the magnetic field distribution of the SUT in real / partial Fourier space
k_x, k_y		spatial wave vector components in x- / y-direction in partial Fourier space
$\boldsymbol{k} = (k_x, k_y)$		vector of the spatial wave vectors in x- / y-direction in partial Fourier space
$k = \sqrt{k_x^{\,2} + k_y^{\,2}}$		modulus of the vector of the spatial wave vectors
K_{u}, K_{d}		perpendicular anisotropy constant, magneto-static energy density

Symbol	Corresponding uncertainty (if applicable)	Description
$m(x,y)$ / $m(k_x,k_y)$		normalized magnetization distribution in real / Fourier space
$M^{\text{eff}}(x,y,z)$ / $M^{\text{eff}}(\boldsymbol{k},z)$		effective magnetic charge pattern in real / Fourier space
M_{S}	uM_{S}	saturation magnetization
m_{S}	um_{S}	magnetic moment per unit area
M_{tip}		tip magnetization orientation, "up" or "down"
$Nx,\ Ny$		pixel number in x- / y-direction
Q	uQ	tip quality factor
$\sigma^{\text{eff}}(x,y)$ / $\sigma^{\text{eff}}(\boldsymbol{k})$		effective magnetic charge distribution in real / partial Fourier space
$Sx,\ Sy$		scan size in x- / y-direction
T		environmental temperature
$\theta,\ \varphi$	$u\theta,\ u\varphi$	canting angles of the cantilever in the setup in polar coordinates
W		sensor sensitivity function
x,y		in-plane scan spatial coordinates
z	uz	tip–sample distance

4 General

4.1 Measurement principle, general

Scanning magnetic field sensors measure either the total stray field amplitude or one or several components of the magnetic field vector distribution of a sample under test (SUT), such as, for example, the perpendicular field component $h_z(x,y,z)$ [5][10][11][12][13][14][15][16]. For the following, we assume that the sensor is scanned over the SUT in an x-y-plane at a constant height z. At any position of the scanning system (x,y,z), the sensor signal is detected with a detection unit and further processed by an analysis system.

$$s(x,y,z) = D\int^{\text{sensor area}} h_z(x+x', y+y', z)\cdot w(x', y')\,\mathrm{d}x'\mathrm{d}y'$$

transition to partial Fourier space: $(x,y,z) \rightarrow (k_x,k_x,z)$

$$S(k_x,k_x,z) = D\cdot W^*(k_x,k_x)\cdot H_z(k_x,k_x,z)$$

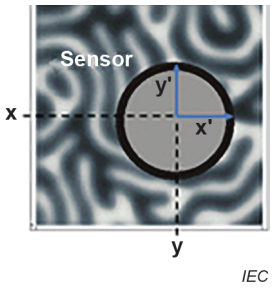

Figure 2 – Field measurement with finite-size sensors

NOTE The signal of a linear finite size sensor at a position (x,y) and at a distance z above a sample surface can be calculated as a weighed ($w(x',y')$) correlation integral over its active area, thus accounting for local sensor sensitivity differences. The analysis system has an additional impact described by a factor D. In partial Fourier space, the correlation integral becomes a multiplication, W^* denotes the complex conjugate of W.

The measurement produces 2D-signal distributions in the (x,y) plane at a measurement height z, $s(x,y,z)$, as a function of the sensor position. When the typical dimensions of the magnetic structures of the SUT show the same order of magnitude as the extension of the probe, the finite sensor size becomes relevant. For certain sensors, the impact of the finite sensor dimensions can be described as a convolution between the sample stray field and the sensor sensitivity function. This document describes a process for the calibration of such sensors that covers the properties of the detection and analysis electronics as well as the contributions of the sensor sensitivity distribution. The sensor is assumed to detect only the magnetic field component perpendicular to the effective sensor plane. Under these assumptions, the measurement process can be described as follows.

The combined influence of the detection unit and analysis system is considered by a factor D, the instrument sensitivity. The additional impact of the finite sensor dimensions with local sensitivity $w(x',y')$ is described by the correlation integral in Figure 2 (right side). For constant height measurements, it is feasible to perform a partial Fourier transform of the coordinates in the sample plane: $(x,y,z) \rightarrow (k_x,k_y,z)$ and thus $h_z \rightarrow \mathcal{F}(h_z(x,y,z)) \equiv H_z(k_x,k_y,z)$. In the partial Fourier space, the correlation integral in the first line in Figure 2 becomes a multiplication with the complex conjugate (marked by the asterisk in Figure 2) of the sensitivity function W (Figure 2 (right side)). In line with the scientific practice, the correlation process is referred to as convolution in this document and the inverse process is referred to as deconvolution. If a sample with a known magnetic field distribution is measured (reference sample), the instrument can be calibrated by a deconvolution of the measured signal S with the known field data H_z, resulting in the frequency and measurement height dependent instrument calibration function (ICF):

$$F^{\mathrm{ICF}}(k_x,k_y,z) = D\cdot W^*(k_x,k_y).$$

Vice versa, a calibrated measurement is achieved by deconvolving the measured data S with the F^{ICF}. For noise free data without zeros in the denominator, the deconvolution steps used in the calibration process and in the calibrated measurement could be done by a simple division in Fourier space. In general, however, for real and therefore noisy data, the deconvolution steps represent inverse ill-posed problems. Therefore, in practice, a regularized deconvolution process needs to be employed. Here, a pseudo-Wiener filter [17] and the L-curve method [18]

to determine the ideal regularization parameter are used to ensure a physically reasonable result.

4.2 Application to scanning systems, discretization

Standard MFM systems do not perform a continuous measurement but rather sample a discrete raster image of the MFM observation variable. For discrete measurement data, it is appropriate to proceed to a fully discrete description of the imaging process, where all 2D data are discretized with the same pixel size $\Delta A = \Delta x \times \Delta y$. In consequence, the above discussed correlation integral then becomes a sum and the above discussed Fourier transform is replaced by a discrete Fourier transform (DFT):

In real space: $$s(i,j,z_0) = D\sum_{k,l} w(k,l)\cdot h_z(i+k, j+l, z_0)\cdot \Delta A \quad (1)$$

In Fourier space: $$S(m,n,z_0) = D\cdot W^*(m,n)\cdot H_z(m,n,z_0) \quad (2)$$

In the following, all formulas are to be understood as discrete representations. For the ease of the discussion, the pixel indices i, j, k, l, m, n are replaced with their assigned spatial or wavevector coordinates, i.e. $i \rightarrow i\cdot\Delta x \triangleq x$, $j \rightarrow j\cdot\Delta y \triangleq y$, $k \rightarrow k\cdot\Delta x \triangleq x'$, $l \rightarrow l\cdot\Delta y \triangleq y'$, $m \rightarrow m\cdot\Delta kx \triangleq kx$, $n \rightarrow n\cdot\Delta ky \triangleq ky$, where $\Delta kx = 2\pi/(N_x\cdot\Delta x)$ and $\Delta ky = 2\pi/(N_y\cdot\Delta y)$.

NOTE In dynamic mode measurements, the gradient of the force acting on the tip is detected. As a consequence, the spatial DC-component of the magnetic field cannot be measured.

4.3 Preparation of the measurement setup

In all following steps, it is assumed that a cantilever chip is mounted to the MFM via a probe assembly, and all necessary steps are performed to detect the cantilever oscillation. This requires the alignment of a light pointer signal. The cantilever excitation frequency is set to an adequate value for MFM detection, as described by the manufacturer. The analysis electronics detects the phase shift signal of the oscillating cantilever as a function of the cantilever position (x,y,z) as provided by the x-y- and z-scanner. Phase shift images are taken in a measurement plane at constant height mode, i.e. in a plane parallel to the sample surface.

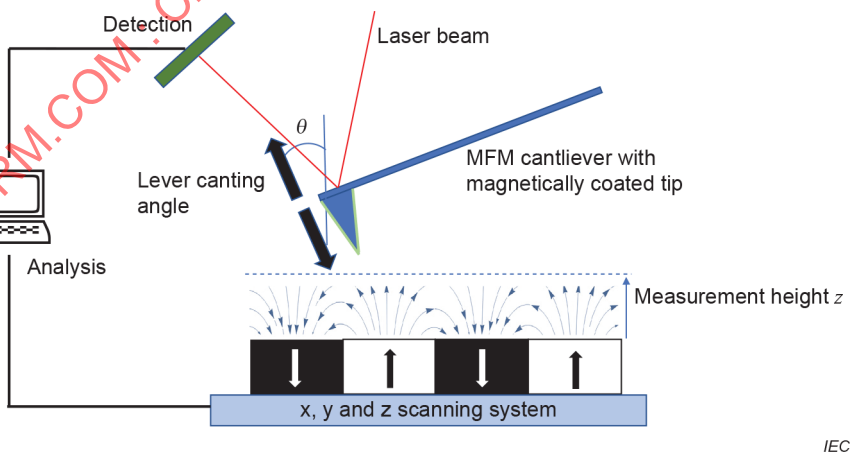

Figure 3 – Schematic MFM setup

4.4 Measurement principle, MFM

4.4.1 General

In the case of MFM, the probe that detects the stray field is a magnetically coated tip attached to an oscillating cantilever, see Figure 3. We here discuss the case of dynamic mode magnetic-

force microscopy in constant height mode where the phase shift of the cantilever oscillation is analysed by a signal detector and a signal analysis system. While an MFM probe tip is a 3D-object, it can be described by the formalism of 4.1 since its sensing properties can be fully described by its emerging stray field gradient distribution in the measurement plane.

4.4.2 Field detection process

For a magnetic sample with a field distribution $H_z^{\text{sample}}(\boldsymbol{k},z)$ at a distance z from the sample surface, it can be shown that in the partial Fourier space the MFM phase shift (in radian) at this measurement height z can be calculated via the following relation:

$$\Delta f(\boldsymbol{k},z) = -\frac{2\mu_0 Q}{C}\cdot F^{\text{LCF}}(\boldsymbol{k},\theta,\varphi,A_{\text{osc}})\cdot H_z^{\text{sample}}(\boldsymbol{k},z)\cdot\frac{\partial H^*_{z,\text{tip}}(\boldsymbol{k},z)}{\partial z} \quad (3)$$

$\frac{\partial H^*_{z,\text{tip}}(\boldsymbol{k},z)}{\partial z}$ is the z-derivative of the z-component of the tip magnetic field, $k=\sqrt{k_x^2+k_x^2}$ and $\boldsymbol{k}$ = (k_x,k_y). Q is the quality factor of the oscillating cantilever with a stiffness C. The factor $F^{\text{LCF}}(\boldsymbol{k},\theta,\varphi,A_{\text{osc}})$, the lever correction function LCF, accounts for the influence of the canting angle of the cantilever relative to the surface normal, θ, and relative to the scan x-axis, φ, as well as for the finite oscillation amplitude A_{osc} of the tip at the measurement height z. Details can be found in Annex A.

NOTE The quality factor Q of the oscillating cantilever at typical measurement heights z can differ from the quality factor found at large distances from the sample surface. The same holds for the oscillation amplitude A_{osc}.

From the above relation we find the functions F^{ICF}, W and D as

$$F^{\text{ICF}}(\boldsymbol{k},C,Q,\theta,\varphi,A_{\text{osc}}) = -\frac{\mu_0 Q}{C}\cdot F^{\text{LCF}}(\boldsymbol{k},\theta,\varphi,A_{\text{osc}})\cdot\frac{\partial H^*_{z,\text{tip}}(\boldsymbol{k},z)}{\partial z} \quad (4)$$

$$D(C,Q) = -\frac{2\mu_0 Q}{C}, \qquad W^*(\boldsymbol{k},z) = \frac{\partial H^*_{z,\text{tip}}(\boldsymbol{k},z)}{\partial z}\ . \quad (5)$$

The factor $F^{\text{LCF}}(\boldsymbol{k},\theta,\varphi,A_{\text{osc}})$ is specific for the MFM imaging process with an oscillating tip and thus not included in the general discussion of 4.2.

4.4.3 Lever correction function F^{LCF}

MFM detects the stray field component parallel to the oscillation direction of the tip along the tip axis. However, the tip is typically canted with a canting angle θ and the cantilever may be rotated with respect to the x-axis by an angle φ. Thus, the measured stray field component deviates from H_z. Additionally, the finite oscillation amplitude A_{osc} leads to an averaging over the measured field along the tip oscillation path. Both contributions can be taken into account in the partial Fourier space by a lever correction function F^{LCF} [19]:

$$F^{\text{LCF}}(\boldsymbol{k},\theta,\varphi,A_{\text{osc}}) = \left(-\frac{1}{k}\boldsymbol{n}\,\nabla_{\boldsymbol{k}}\right)^2\cdot\sum_{m=0}^{\infty}\frac{1}{m!(m+1)!}\left(\frac{\chi}{2}\right)^{2m}$$

with χ = $A_{\text{osc}}\,\boldsymbol{n}\nabla_{\boldsymbol{k}}$.

Here $\boldsymbol{n}$ is the normalized vector parallel to the tip axis,

$$\boldsymbol{n} = \left(\sin(\theta)\cos(\varphi), \sin(\theta)\sin(\varphi), \cos(\theta)\right),$$

and $\nabla_{\boldsymbol{k}}$ is the gradient in Fourier space

$$\nabla_{\boldsymbol{k}} = \left(ik_x, ik_y, -k\right).$$

In the sum, terms with m > 4 typically can be neglected.

Figure 4 shows an example of the real part of an F^{ICF} for different values of the oscillation amplitude A_{osc}. The F^{LCF} part determines the change in the measured amplitude of the phase shift $\Delta\varphi$.

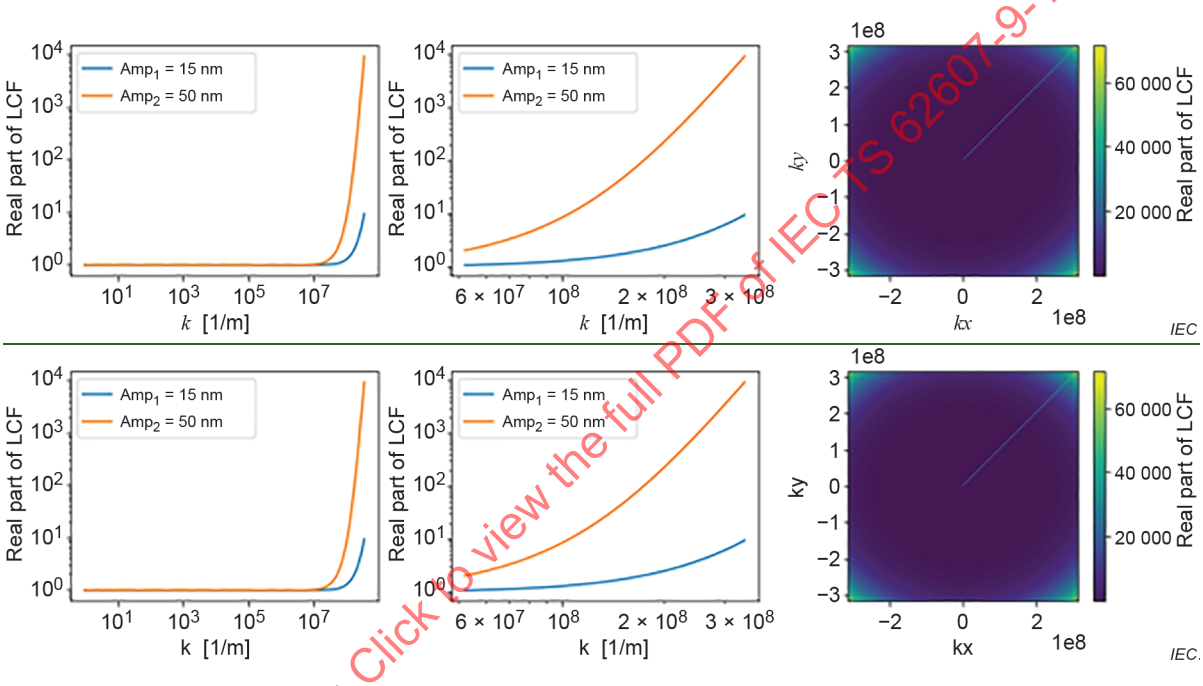

NOTE Double-logarithmic line plots of the F^{LCF} real part (left and centre) and 2D plot of the F^{LCF} (real part, right) for θ = 7°, φ = 0°. The line plots show the F^{LCF} for plot A_{osc} = 15 nm (blue line) and A_{osc} = 50 nm (orange line). Both lines are plotted along the direction shown as a blue line in the 2D plot. The centre image shows an enlarged section of the left plot.

Figure 4 – Lever correction function (F^{LCF}) in Fourier space

The F^{LCF} accounts for the increase of the measured phase signal $\Delta\varphi$ due to the cantilever oscillation. As can be seen in Figure 4, the signal enhancement is larger for smaller structures (larger wavevector k) and grows disproportionally with increasing oscillation amplitude.

NOTE 1 The amplitude induced signal enhancement typically cannot be exploited to increase the systems measurement sensitivity. For real measurements, maintaining a minimum distance z_{min} of the tip to sample surface avoids Van-der Waals interactions between the tip and the sample. This needs higher tip–sample distances for higher oscillation amplitudes.

Figure 5 shows the F^{LCF} multiplied with the z and $\boldsymbol{k}$-dependent field transfer function that describes the decay of the magnetic field for two oscillation amplitudes A_{osc1} = 15 nm (orange line) and A_{osc2} = 15 nm (blue line) for z_{min} = 30 nm [16] and thus for minimum possible tip–sample distances z_1 = 45 nm and z_2 = 80 nm. The data are normalized with respect to the signal z_0 = 30 nm and in the limit of zero oscillation amplitude. In this example, the signal increase by the amplitude enhancement is overcompensated by the signal loss due to the higher distance, for all $\boldsymbol{k}$-values. On the other hand, lower oscillation amplitudes lead to a lower signal-to-noise

ratio of the measurement. Therefore, the oscillation amplitude can be individually optimized by balancing measurement noise and sensitivity for the respective measurement system.

NOTE 2 The F^{LCF} correction becomes relevant for structure sizes in the order of magnitude of the cantilever oscillation or below.

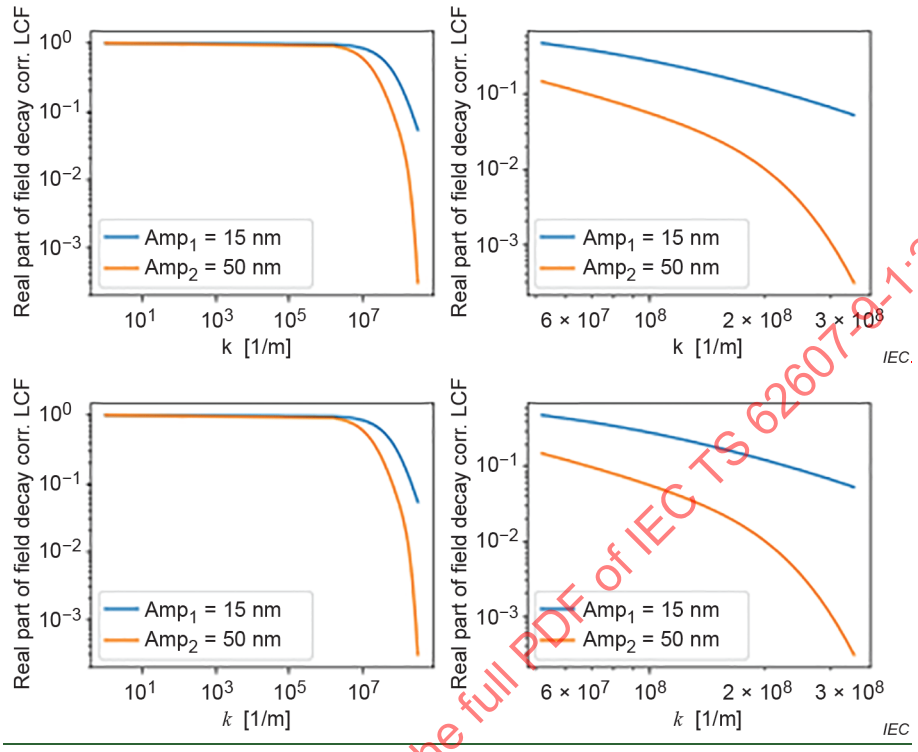

NOTE Double logarithmic line plots of the F^{LCF} real part multiplied with the field decay factor for oscillation amplitudes A_{osc} = 15 nm (blue line) and A_{osc} = 50 nm (orange line) for tip–sample distances of z_1 = 45 nm and z_2 = 80 nm, respectively (z_{min} = 30 nm + tip oscillation amplitude), normalized with respect to the signal z_0 = 30 nm in the limit of zero oscillation amplitude.

Figure 5 – Lever correction function (F^{LCF}) and distance losses

4.4.4 Effective magnetic charge density of the tip

In the case of MFM, the sensor sensitivity function $W^*(\boldsymbol{k},z)$ only comprises static magnetic properties of the tip. All other cantilever and instrument related contributions are included in $D(C,Q)$ and $F^{LCF}(\boldsymbol{k},\theta,\varphi,A_{osc})$. The $W^*(\boldsymbol{k},z)$ can equivalently be described in terms of the tip stray field or the tip's effective magnetic charge density at the tip apex:

$$W(\boldsymbol{k},z) = \frac{\partial H_{z,\mathrm{tip}}(\boldsymbol{k},z)}{\partial z} = -k\,H_{z,\mathrm{tip}}(\boldsymbol{k},z) = \frac{1}{2}k\cdot\sigma^{*}(\boldsymbol{k}) \tag{7}$$

4.4.5 Characteristics of the MFM F^{ICF}

The instrument calibration function F^{ICF} contains all information necessary to describe the MFM imaging process by a convolution with the magnetic field and vice versa to convert MFM phase-shift images to magnetic field distributions in SI units by a deconvolution of the measured phase shift signal. The F^{ICF} can be displayed in real space (RS) or in partial Fourier space (PFS), see Figure 6.

- Partial Fourier space representation (Figure 6, left side).

  The MFM imaging process is linear in the partial Fourier space. The F^{ICF} in partial Fourier space describes the weighing factor for field contributions with different $\boldsymbol{k}$-vectors. The F^{ICF}

approaches zero for large and small $\boldsymbol{k}$-vectors and has a maximum for k-values comparable to the spatial extension of the tip.

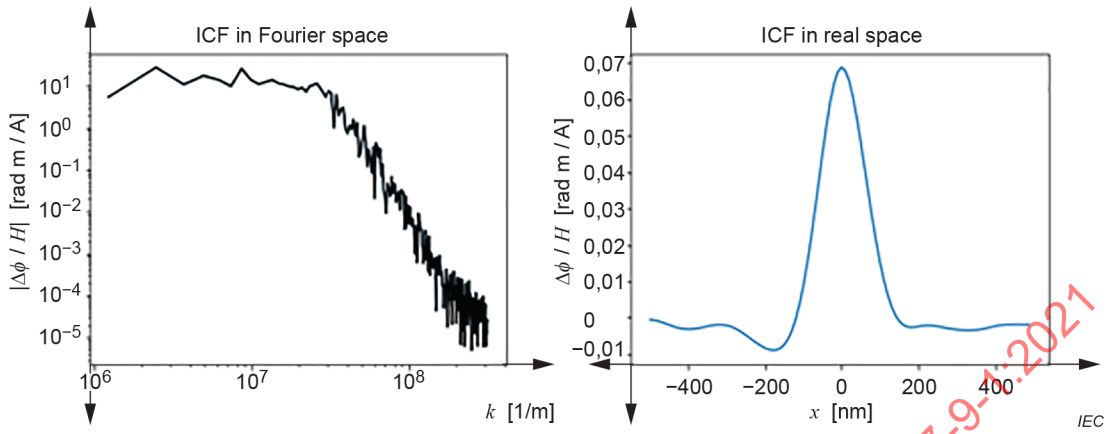

NOTE Representations of the F^{ICF} of a commercial MFM tip, calculated using a calibration sample with band domain pattern.

Figure 6 – Instrument calibration function (F^{ICF}) in real and Fourier space. Line plots of the partial Fourier space (absolute value, left) and real space (right).

- Real space representation (Figure 6, right side).

  The real space representation of the F^{ICF} illustrates the broadening aspect of the imaging process, i.e. the effective spatial extension of the sensor. If $D(C,Q)$ and $F^{\mathrm{LCF}}(\boldsymbol{k},\theta,\varphi,A_{\mathrm{osc}})$ are known, the real space representation of the effective magnetic charge distribution of the tip, $\sigma(x,y,z)$, and the tip stray field as well as its gradients can be calculated in SI units. Both distributions can be used for a plausibility test of the calculated F^{ICF} and to assess the impact of the tip magnetic field on the sample under test.

In the following, F^{ICF} is used without further labelling for its real space and Fourier space representations, discernible from context and parameter set (x,y,z) or $(\boldsymbol{k},z)$.

4.4.6 Concept of calibration by deconvolution

The determination of the F^{ICF} from the measurement $\Delta\varphi^{\mathrm{ref}}(\boldsymbol{k},z)$ of a reference sample (ref) with a known stray field distribution $H^{\mathrm{ref}}(\boldsymbol{k},z)$ as well as calculation of the field distribution $H_z^{\mathrm{SUT}}(\boldsymbol{k},z)$ of a sample under test (SUT) from the measured phase shift data $\Delta\varphi^{\mathrm{SUT}}(\boldsymbol{k},z)$ requires a deconvolution step, which, in principle, is mathematically described in the form of a division in the Fourier space:

$$F^{\mathrm{ICF,ref}}(\boldsymbol{k},z)=\frac{\Delta\varphi^{\mathrm{ref}}(\boldsymbol{k},z)}{H_z^{\mathrm{ref}}(\boldsymbol{k},z)} \quad \text{and} \quad H_z^{\mathrm{SUT}}(\boldsymbol{k},z)=\frac{\Delta\varphi^{\mathrm{SUT}}(\boldsymbol{k},z)}{F^{\mathrm{ICF,ref}}(\boldsymbol{k})}\,. \tag{8}$$

The deconvolution of measured phase shift with the $F^{\mathrm{ICF,ref}}$ requires the use of the same magnetic probe under the identical experimental conditions as used in the ICF calibration step with a reference sample. Alternatively, the same magnetic probe can be used with varied experimental conditions and thus a modified $F^{\mathrm{ICF,SUT}}$. The ICF depends linearly on the instrument dependent part $D(C,Q)$ and $F^{\mathrm{LCF}}(\boldsymbol{k},\theta,\varphi,A_{\mathrm{osc}})$ as well as on its constituents C, Q and ΔA. Under changing instrument parameters, the ICF therefore transforms like

$$F^{\mathrm{ICF,SUT}} = -2\mu_0 \frac{Q^{\mathrm{SUT}}}{C^{\mathrm{SUT}}} \cdot F^{\mathrm{LCF}}\left(\boldsymbol{k}, \theta^{\mathrm{SUT}}, \varphi^{\mathrm{SUT}}, A_{\mathrm{osc}}^{\mathrm{SUT}}\right) \cdot \frac{\partial H_{\mathrm{tip}}^{*}(\boldsymbol{k}, z)}{\partial z}$$

$$= \frac{\frac{Q^{\mathrm{SUT}}}{C^{\mathrm{SUT}}} \cdot F^{\mathrm{LCF}}\left(\boldsymbol{k}, \theta^{\mathrm{SUT}}, \varphi^{\mathrm{SUT}}, A_{\mathrm{osc}}^{\mathrm{SUT}}\right)}{\frac{Q^{\mathrm{ref}}}{C^{\mathrm{ref}}} \cdot F^{\mathrm{LCF}}\left(\boldsymbol{k}, \theta^{\mathrm{ref}}, \varphi^{\mathrm{ref}}, A_{\mathrm{osc}}^{\mathrm{SUT}}\right)} \cdot F^{\mathrm{ICF,ref}}$$

Consequently, no knowledge about the instrument parameters is required when a calibration and a subsequent calibrated measurement of a sample under test are performed with unchanged device control parameters, since then $F^{\mathrm{ICF,SUT}} = F^{\mathrm{ICF,ref}}$. All parameters are then implicitly included in the ICF. On the other hand, if parameters are changed between calibration and calibrated measurement, the ICF is no longer valid and thus has to be adapted.

For example, if the polar canting angle changes from θ_1 during calibration measurement to θ_2 when the sample under test is measured, the ICF transfers like:

$$F^{\mathrm{ICF}}(\boldsymbol{k}, z, \theta_2, \varphi) = F^{\mathrm{ICF}}(\boldsymbol{k}, z, \theta_1, \varphi) \frac{F^{\mathrm{LCF}}(\boldsymbol{k}, \theta_2, \varphi, A_{\mathrm{osc}})}{F^{\mathrm{LCF}}(\boldsymbol{k}, \theta_1, \varphi, A_{\mathrm{osc}})} .$$

Accordingly, for the quantitative stray field calculation, the calculated data shall be corrected with the reciprocal factor:

$$H_z^{\mathrm{SUT}}(\boldsymbol{k}, z) = \frac{\Delta\varphi^{\mathrm{SUT}}(\boldsymbol{k}, z)}{F^{\mathrm{ICF}}(\boldsymbol{k}, z, \theta_1, \varphi)} \cdot \frac{F^{\mathrm{LCF}}(\boldsymbol{k}, \theta_1, \varphi, A_{\mathrm{osc}})}{F^{\mathrm{LCF}}(\boldsymbol{k}, \theta_2, \varphi, A_{\mathrm{osc}})} .$$

Similar relations hold for the other parameters.

4.4.7 Regularized deconvolution approach

For real, noisy measurement data, the deconvolution step described in Formula (8) represents an ill-posed problem. Noise in the denominator functions would be amplified and the quotient would diverge where the divisor equals zero. Therefore, the deconvolution needs to be regularized to achieve physically meaningful results which are robust against noise.

In this document, a regularization process is implemented which applies a pseudo-Wiener filter with a regularization parameter α:

$$F^{\mathrm{ICF,ref}}(\boldsymbol{k}, z) = \Delta\varphi^{\mathrm{ref}}(\boldsymbol{k}, z) \frac{H_z^{\mathrm{ref}*}(\boldsymbol{k}, z)}{\left|H_z^{\mathrm{ref}}(\boldsymbol{k}, z)\right|^2 + \alpha} \quad , \quad H_z^{\mathrm{SUT}}(\boldsymbol{k}, z) = \Delta\varphi^{\mathrm{SUT}}(\boldsymbol{k}, z) \frac{F_\alpha^{\mathrm{ICF,ref}*}(\boldsymbol{k}, z)}{\left|F_\alpha^{\mathrm{ICF,ref}}(\boldsymbol{k}, z)\right|^2 + \alpha} \qquad (9)$$

The outcome of the regularization depends critically on the regularization parameter. Here, the optimum regularization parameter α is calculated by the L-curve method [18].

Hereafter, the pseudo-Wiener filter in combination with the L-curve method is used as the default deconvolution process.

4.5 MFM setup key control characteristics

4.5.1 General

The relevant data sets for calibrated field measurements are the reference sample's raw data distribution, here phase shift data $\Delta\varphi^{ref}$, and its magnetic field distribution H_z^{ref}, the ICF calculated from it, the measured raw data distribution of the sample under test, here the phase shift distribution $\Delta\varphi^{SUT}$, and the magnetic field distribution H_z^{SUT} calculated from it. Furthermore, setup parameters that are not or cannot be kept constant need to be controlled. Table 1 summarizes all relevant KCCs. Standardized approaches to extract quantitative data for the relevant setup parameters are discussed in 4.5.2 to 4.5.9.

Table 1 – MFM setup key control characteristics

Key control characteristics	Identifier	Typical value	Comment	Category
cantilever spring constant	C	5 N/m	supposed to be constant	instrument parameters
tip quality factor	Q	250 (ambient conditions) 10 000 (UHV)	shall be measured with a reference sample and sample under test measurement. Depends on distance to the sample surface	
cantilever oscillation amplitude	A_{osc}	20 nm	shall be small compared to typical structure sizes	
measurement height	z	60 nm	lift height + oscillation amplitude in approached state	
scan size pixel size pixel number	$Sx \times Sy$ $\Delta x \times \Delta y$ $Nx \times Ny$	5,11 µm × 5,11 µm 10 nm × 10 nm 512 × 512	set by user	
scanning speed		5 µm/s to 10 µm/s	Slow speed = lower noise, but also more drift	
cantilever canting angles in the setup	θ φ	10° 0°	from manufacturer set by user	
tip magnetization orientation	M_{tip}	"up" / "down" "+" / "−"	can be set by magnetizing the tip in an external magnetic field	
z-component of the magnetic field distribution of the reference sample	$H_z^{\mathrm{ref}}(x,y,z)$ / $H_z^{\mathrm{ref}}(\boldsymbol{k},z)$			reference sample
deconvolution approach used for ICF determination and for the calibrated measurement		"default" or user default = pseudo-Wiener filter with L-curve criterion for optimized regularization	Deconvolution approach used for ICF determination and for the calibrated measurement	analysis technique
reference sample raw data distribution, here phase shift data in real / partial Fourier space	$\Delta\varphi^{\mathrm{ref}}(x,y,z)$ / $\Delta\varphi^{\mathrm{ref}}(\boldsymbol{k},z)$			measurement data
SUT raw data distribution, here phase shift data in real / partial Fourier space	$\Delta\varphi^{\mathrm{SUT}}(x,y,z)$ / $\Delta\varphi^{\mathrm{SUT}}(\boldsymbol{k},z)$			
instrument calibration function	$F^{\mathrm{ICF}}(x,y,z)$ or $F^{\mathrm{ICF}}(\boldsymbol{k},z)$			calculated data
z-component of the magnetic field distribution of the sample under test	$H_z^{\mathrm{SUT}}(x,y,z)$ / $H_z^{\mathrm{SUT}}(\boldsymbol{k},z)$			

4.5.2 Cantilever spring constant C

The cantilever spring constant is supposed to be constant. If C is determined, this shall be carried out as described in ISO 11775:2015 [21].

4.5.3 Cantilever resonance quality factor Q

The cantilever resonance quality factor Q can be obtained from the resonance curve of the tip as shown in Figure 7. From this curve, Q is calculated as $Q = f_0 / \Delta f$, where f_0 is the resonance frequency, Δf is the full width at 0,707 of the maximum amplitude [22]. Q is usually not stable and needs to be calculated for each calibration and calibrated measurement and at the actual measurement height. Q can vary significantly (approximately 20 %) at different measurement heights (from 100 µm to 100 nm).

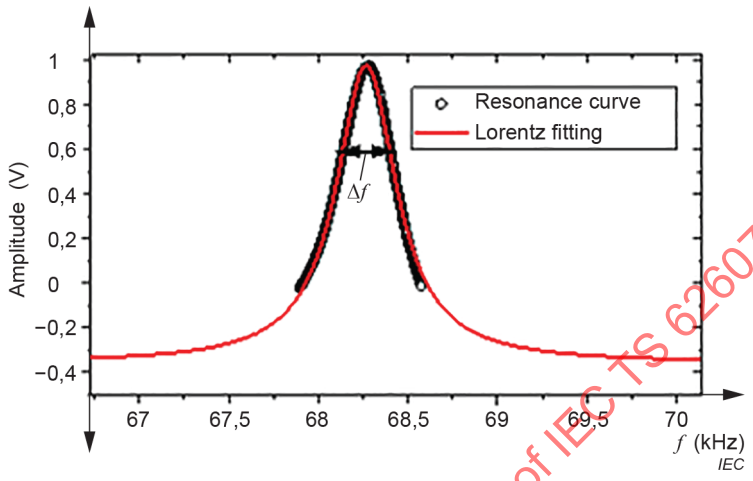

Figure 7 – Typical resonance curve of a cantilever

4.5.4 Sensitivity of the detection and analysis electronics

If the oscillation amplitude of the cantilever is not given in nanometre units, the deflection data shall be converted to nanometres (typically from volts) after a calibration of the signal detector. This requires measuring a deflection–distance curve (static) or amplitude–distance (dynamic) for the cantilever using a bare hard substrate. Thereby the sensitivity of the oscillation detection electronics is traced back to the tip–sample distance and thus to the z-piezo calibration. The deflection–distance curve is typically measured on a silicon substrate. An exemplary curve is shown in Figure 8. From the linear fitting of the curve (blue line), the sensitivity of the cantilever can be calculated (in the example in nm/V). This value shall be used to convert the deflection data into nanometres and vice versa, to set a specific oscillation amplitude in nanometres. The cantilever sensitivity is assumed to be stable. Since the measurement of a deflection–distance curve is potentially invasive, the sensitivity shall be measured after the completion of all measurements.

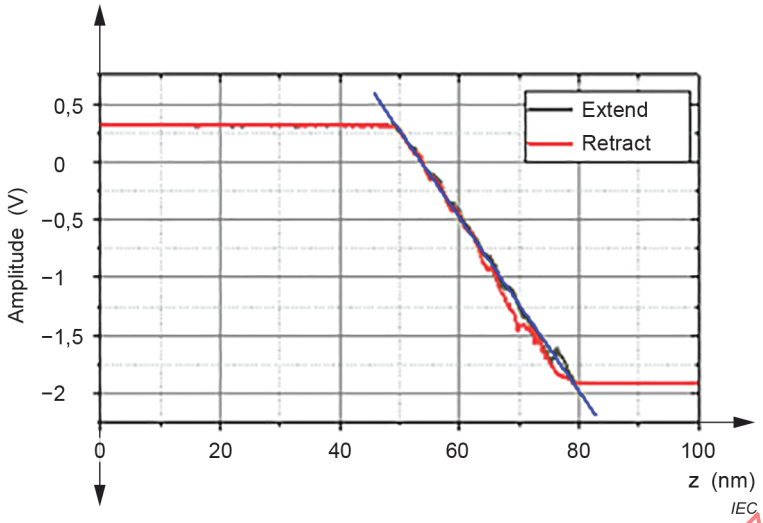

Red curve: typical force plot of a cantilever.

Blue curve: linear transition region.

Figure 8 – Typical amplitude–distance plot of a cantilever with the linear transition region indicated

4.5.5 Measurement height

The measurement height is defined as the distance of the centre of the tip apex oscillation from the sample surface. Therefore, the measurement height z results from adding the oscillation amplitude A_0 of the approached tip to the nominal lift height z^{lh} of the MFM measurements:

$$z = A_0 + z^{\mathrm{lh}} .$$

The lift height is set by the user.

NOTE A_0 typically is different from the oscillation amplitude during the constant height measurement A_{osc}.

4.5.6 Scan size, pixel resolution

Scan size $Sx \times Sy$ and pixel resolution Nx, Ny (number of pixels in x and y directions) and thus the pixel sizes Δx and Δy are set by the user.

4.5.7 Canting angle of the cantilever in the setup

The canting of the lever can be described by two angles in polar coordinates. The azimuthal tilt φ and the polar angle θ.

θ is a property of the probe assembly and describes the tilt of the tip axis relative to the sample surface normal vector. It is given by the manufacturer of the probe assembly. It typically is chosen as about 10°.

φ describes the cantilever orientation relative to the x-coordinate of the image to be analysed. Typical values are 0° (horizontal scanning direction) and 90° (vertical scanning direction).

4.5.8 Magnetization orientation of the tip

Some reference samples, like band domain samples, do not allow an unambiguous determination of the sign of the tip effective magnetic charge distribution $\sigma(\boldsymbol{k})$ and thus the ICF. For such reference samples the orientation of the tip shall be measured by other means or set by aligning the tip magnetization in a sufficiently strong homogeneous external magnetic field.

4.5.9 Regularized deconvolution

The default regularized deconvolution approach is the application of a pseudo-Wiener filter in combination with the L-curve criterion. If no user-specific optimization approach for α is used and described, the optimum regularization parameter α shall be calculated by the L-curve method [18].

Any other feasible regularization approach is permitted, but the process shall be protocolled and documented and shall be declared together with the F^{ICF} and the resulting H_z^{SUT}.

4.6 Ambient conditions during measurement

Ambient conditions key control characteristics are summarized in Table 2.

The temperature T shall be kept stable to ±1 K during the measurement since changes of temperature lead to thermal drift that can impact the precision of the positioning system.

Humidity H shall be controlled to (50 ± 4) % relative humidity and humidity and temperature shall be documented including their variability during the measurement process.

Table 2 – Ambient conditions key control characteristics

Key control characteristic	Identifier	Typical value	Comment
temperature	T	(20 ± 1) °C	Shall be kept within the specified range. The impact on the measurement depends on the setup.
humidity	H	(50 ± 4) %	Shall be kept within the specified range. The impact on the measurement depends on the setup.

4.7 Reference samples

4.7.1 General

The tip calibration requires a reference sample. Reference samples are samples with well-known or calculable stray field distributions. They are used to determine the ICF. They (a) shall be stable over time and shall not be altered by the stray field of the scanning magnetically coated tip and (b) shall inversely not alter the magnetization of the tip. The calibration is done in Fourier space and the ICF only contains information for $\boldsymbol{k}$-vectors that are included in the reference samples. Therefore, the reference sample shall be chosen in regard to its Fourier spectrum and shall be suitable for the sample under test, i.e. shall cover the spatial Fourier spectrum of the SUT's magnetic field distribution.

4.7.2 "Well-known" and calculable reference sample

Any sample fulfilling the requirements above can be made a "well known" reference sample if it (i) has a well-known magnetization pattern with a calculable magnetic field distribution or if (ii) its magnetic field distribution is stable and has been quantitatively characterized by other means. High resolution quantitative stray field measurements are, for example (to a lesser extent), available in the form of scanning nitrogen-vacancy-centre magnetometry [23]. Patterned samples allow a spatial alignment of characterization and calibration measurements.

4.7.3 Band domain patterns as self-referencing calibration samples

Thin film samples with band domain patterns do not per se have a well-known magnetization pattern. However, it is possible to guess the underlying magnetization pattern from the measured MFM image without detailed knowledge on the yet to be calibrated probe if the

magnetic properties of the sample material are known. This is discussed here for the example of a Co/Pt multilayer film with perpendicular anisotropy.

In zero field the magnetization of the multilayer collapses into a band domain pattern with an average domain width in the sub-micrometre range. The domain pattern depends on the exact layer structure, which is related to the manufacturing conditions and cannot be controlled to a sufficient degree to be dependable. Nevertheless, if the layer structure is designed and manufactured properly, the multilayer shows well-defined up and down magnetized band domains separated by transition regions with a width of the transition of the order of 10 nm. As the band domain pattern of the reference sample develops homogeneously across the whole sample surface, a specification of the measurement region is not necessary if the size of total scanned area is kept constant.

The specific multilayer film discussed here as an example was prepared by magnetron sputtering with the following layer architecture:

Pt(2 nm)/[(Co(0,4 nm)/Pt(0,9 nm)]100/Pt(5 nm)/Ta(5 nm)/SiOx/Si(100).

The total thickness of the magnetic layer is d = 130 nm and – owing to the interface anisotropy of the thin Co layers – the film develops a magnetic anisotropy perpendicular to the surface. The band domain pattern shows an average domain width of 170 nm. Global magnetization measurements determined the magnetic moment per area m_S and thus the saturation magnetization to be $M_S = m_S/d$ = 500 kA/m (error: ±30 kA/m) and confirm the perpendicular magnetization through a ratio $Q_u = K_u / K_d \geq 2{,}5$ (K_u = 0,4 MJ/m^3 is the perpendicular anisotropy constant, $K_d = ½\mu_0 M_S$ = 0,16 MJ/m^3 is the magnetostatic energy density). The Bloch type domain transition has a width δ_{DW} of about 16 nm.

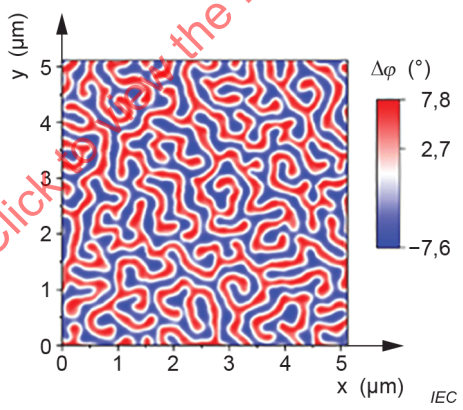

Figure 9 – Band domain reference sample

4.7.4 Detailed stray field calculation procedure for perpendicularly magnetized band domain reference samples

The z-component of the band domain reference sample magnetic field distribution as required for the determination of the ICF shall be calculated by the following procedure:

1) An MFM raw data distribution, here phase shift data, of an area with the required pixel size and number and at a given measurement height z is recorded (Figure 9).
2) Data pre-processing (flattening, background subtraction) is performed.
3) The influence of the lever canting and finite oscillation amplitude is corrected in Fourier space by dividing the AFM phase shift data by the lever correction function F^{LCF} [19].

$$F^{\mathrm{LCF}}\left(\boldsymbol{k},\theta,\varphi,A_{\mathrm{osc}}\right)=\left(-\frac{1}{k}\boldsymbol{n}\nabla_{\boldsymbol{k}}\right)^{2}\cdot\sum_{m=0}^{\infty}\frac{1}{m!(m+1)!}\left(\frac{\chi}{2}\right)^{2m}$$

where $\chi = A_{\mathrm{osc}}\,\boldsymbol{n}\nabla_{\boldsymbol{k}}$.

4) The underlying domain pattern is estimated by a discrimination. The discrimination criterion, a threshold value, is found by assuming that up- and down-magnetized domains show the same raw data amplitude. It results into a normalized $m(x,y)$ distribution, depicting up (+1) and down (−1) domains.

5) Bloch like domain transitions are added by a convolution with a domain wall kernel $k(x,y)$, accounting for the known domain wall type and transition width δ_{DW} [24]. A particular kernel that can be used for Bloch walls is given as [16][25]

$$k\left(x,y\right)=\operatorname{sech}\left(\frac{\pi\sqrt{x^{2}+y^{2}}}{\delta_{\mathrm{DW}}}\right)=\operatorname{sech}\left(\frac{\pi r}{\delta_{\mathrm{DW}}}\right) \tag{10}$$

This leads to domain wall-corrected normalized magnetization distribution $m^{\mathrm{DW}}(x,y)$.

6) For the assumed perpendicular magnetization, the magnetization distribution $m^{\mathrm{DW}}(x,y)$ leads to a surface charge pattern $\sigma^{\mathrm{ref},+}(x,y,z=0) = m^{\mathrm{DW}}(x,y,z=0)\cdot M_{\mathrm{S}}$ at the upper surface of the reference sample and to $\sigma^{\mathrm{ref},-}(x,y,z=-d) = m^{\mathrm{DW}}(x,y,z=-d)\cdot M_{\mathrm{S}}$ at the lower sample surface. The effective surface charge $\sigma^{\mathrm{ref,eff}}$, i.e. the projection of all magnetic charges onto the upper surface of the sample with thickness d is given by [26]

$$\sigma^{\mathrm{ref,eff}}\left(\boldsymbol{k},0\right)=M_{\mathrm{S}}\,m^{\mathrm{DW}}\left(\boldsymbol{k},0\right)\cdot\left(1-e^{-kd}\right) \tag{11}$$

7) The stray field of the $H_z^{\mathrm{ref}}(x,y,z)$ at the measurement height is calculated from $\sigma^{\mathrm{ref,eff}}$ in Fourier space by a multiplication with a z- and $\boldsymbol{k}$-dependent field transfer function:

$$H_z^{\mathrm{ref}}\left(\boldsymbol{k},z\right)=\sigma^{\mathrm{ref,eff}}\left(\boldsymbol{k},0\right)\cdot\frac{e^{-kz}}{2} \tag{12}$$

Table 3 – Stray field estimation key control characteristics

Key control characteristic	Identifier	Typical value	Comment	Category
cantilever oscillation amplitude	A_{osc}	20 nm	for a discussion on the choice of oscillation amplitudes, see 4.4.3	instrument parameters
measurement height	z	60 nm	as close as possible to the surface, but distant enough to avoid van der Waals interaction and contact with surface features	
scan size pixel size pixel number	$Sx \times Sy$ $\Delta x \times \Delta y$ $Nx \times Ny$	5,11 µm × 5,11 µm 10 nm × 10 nm 512 × 512	same as scan size of sample under test	
canting angle of the cantilever in the setup	θ φ	10° 0°	given by the MFM manufacturer set by user	
sample remnant magnetization	M_{S}	500 kA/m	larger M_{S} yield a lower uncertainty due to the higher signal/noise ratio but can enhance unwanted impact on tip magnetization	reference sample parameters

Key control characteristic	Identifier	Typical value	Comment	Category
domain transition type and width	δ_{DW}	16 nm	samples with smaller domain wall transitions show contributions at higher $\boldsymbol{k}$-vectors	
sample thickness	d	some 10 nm	thickness of the magnetic material layer	
deconvolution approach used for F^{ICF} determination		"default" or user defined default = pseudo-Wiener filter and L-curve criterion	Unless the default approach is used, the deconvolution approach shall be documented and protocolled	analysis technique
calibration measurement raw data distribution (phase shift data)	$\Delta\varphi^{ref}(x,y,z)$	typically a few degrees	Signal depends on H_z^{ref} and F^{ICF}	measurement data
calculated magnetic field distribution	$H_z^{ref}(x,y,z)$	typically some 10 kA/m	Depends on reference sample parameters and strongly on measurement height	calcula-ted data

Van-der-Waals forces are present at any distance from the sample but decay rapidly with increasing distance while magnetic forces are long-range. At a distance of 30 nm from the sample surface, magnetic forces can be expected to exceed Van-der-Waals forces by two orders of magnitude [20]. However, in dynamic mode MFM where tip oscillation amplitudes of several tens of nanometres can well occur, Van-der-Waals interactions can play a role in signal generation and impact the measured phase shift signal. Therefore, users are advised to calibrate the oscillation amplitude and choose the measurement height in such a way that even at the lower turning point the tip never comes closer to the surface than 30 nm to avoid artefacts.

To summarize, by applying steps 1) to 7), a stray field distribution is calculated from the calibration measurement itself, employing the known reference sample magnetic parameters. The stray field calculation for band domain pattern-based reference samples requires a control of the key parameters listed in Table 3. The succession of the individual steps involved in the process is summarized and illustrated in Table 4.

Table 4 – Stray field estimation protocol

Step	Action	Illustration	Status
1a	MFM is set up as discussed under 4.4		required
1b	scan and sample parameters are set or monitored	example: z = 60 nm; φ = 0°; Δx = 10 nm; A_{osc} = 20 nm; Δy = 10 nm; δ_{DW} = 16 nm; θ = 10°; M_{tip} : up	required
1c	measurement of the raw data distribution (phase shift data)	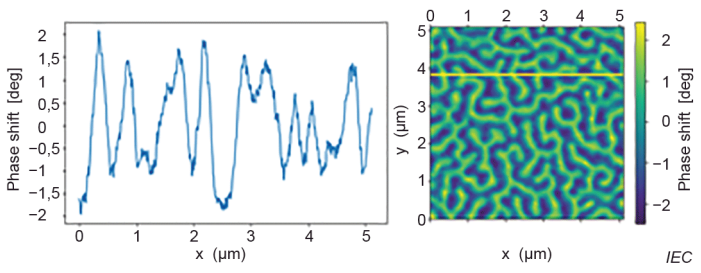	required

Step	Action	Illustration	Status
2	data pre-processing	e.g. levelling	optional
3	correction of lever impact (angle, oscillation amplitude)	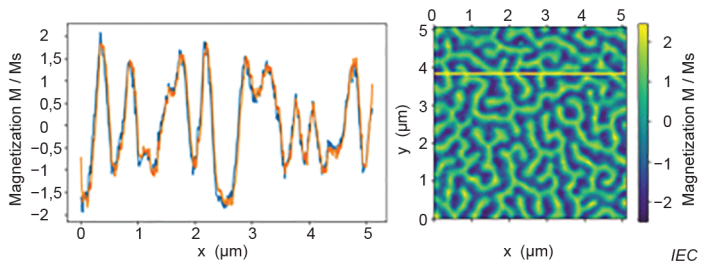	optional
4	normalized magnetization distribution from discrimination	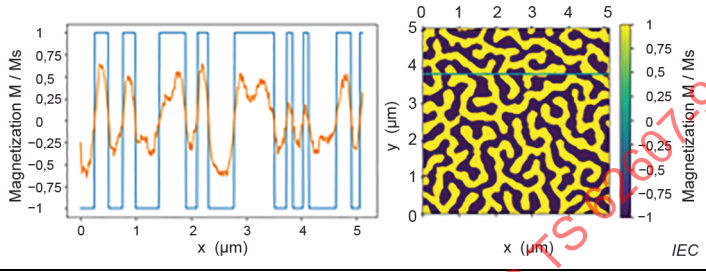	required
5	adding of domain wall transitions	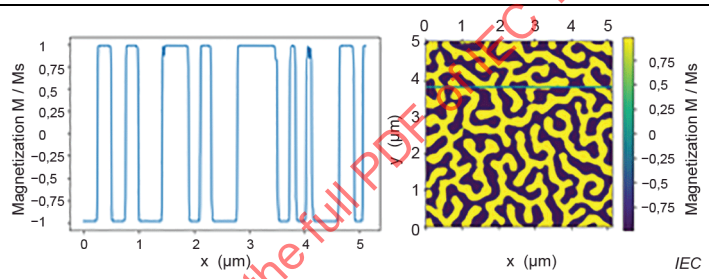	required
6+7	calculation of sample effective charge distribution $\sigma^{ref,eff}$ and of the magnetic field distribution H_z^{ref} at distance z	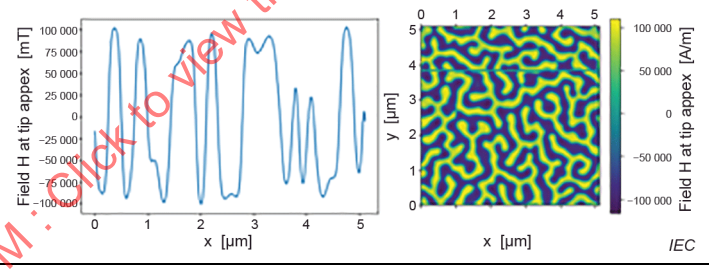	required

5 Measurement procedure for calibrated magnetic field measurements

5.1 Calibrated stray field measurement of a sample under test

The quantification of stray fields by qMFM (quantitative MFM) requires (i) a tip calibration by measuring a reference sample with a known magnetic field distribution H_z^{ref} and (ii) a measurement of the raw data distribution of the SUT.

To ascertain that no unintended changes in the control parameters and of the tip properties have happened during the actual measurement, the standardized sequence of measurement steps is as follows:

measurement of a reference sample

↓

measurement of the sample under test

↓

measurement of the reference sample

5.2 Detailed description of the measurement and calibration procedure

1) MFM setup as discussed under 4.4.
2) Adjustment of probe's oscillation amplitude to a suitable value.
3) Characterization of cantilever resonance quality factor Q at the chosen measurement height (4.5.2).
4) (repeated) Measurement of the MFM raw data distribution (here: phase shift data) of the reference sample with well-adjusted measurement height z and with the required pixel size and number.
5) (repeated) Measurement of the MFM raw data distribution (here: phase shift data) of the sample under test with preferably identical parameters.
6) (repeated) Measurement of the MFM raw data distribution (here: phase shift data) of the reference sample with preferably identical parameters as in step 4).
7) Characterization of cantilever resonance quality factor Q at the chosen measurement height as described under 4.5.3.
8) Calculation of the ICF from steps 4) and 6):
   a) Data pre-processing (flattening, background subtraction) and windowing, partial Fourier transform. If the band domain pattern is used, follow steps 2) to 6) in 4.7.4 to calculate H_z^{ref}.
   b) Selection of either a user defined deconvolution or the default deconvolution approach discussed in 4.5.9.
   c) Calculation of the ICF using the deconvolution approach selected under b).
   d) When applicable, the F^{ICF} data from steps 4) and 6) can be averaged separately using the F^{ICF} data of the repeated measurements from steps 4) and 6).
   e) Check if (averaged) F^{ICF} data from steps 4) and 6) agree within a tolerable margin. If yes, proceed; otherwise repeat the measurements.
   f) (optional) Smooth F^{ICF} either by circular averaging or segmental averaging along concentric rings around k = (0,0).
9) Correction of the F^{ICF} for changed KCCs as discussed under 4.4.6.
10) Calculation of quantitative magnetic field distribution of the sample under test from step 5):
   a) Pre-processing of the measured SUT raw data distribution (flattening, background subtraction) and windowing, partial Fourier transform.
   b) Calculation of the quantitative magnetic field distribution in partial Fourier space from (if applicable: averaged) pre-processed SUT raw data distribution (here: phase shift data) using either a user defined deconvolution or the default deconvolution employing the (if applicable: corrected and if applicable: averaged) F^{ICF} from step 8) or 9).
   c) Inverse Fourier transformation of the quantitative magnetic field distribution.

5.3 Measurement protocol

Table 5 shows the protocol of the measurement procedure

Table 5 – Measurement protocol

Step	Action	Illustration	Status
1	MFM is set up as discussed under 4.4		required
2	adjustment of the cantilever oscillation amplitude	example: A_{osc} = 20 nm	optional
3	measurement of the cantilever quality factor Q using the manufacturer's software	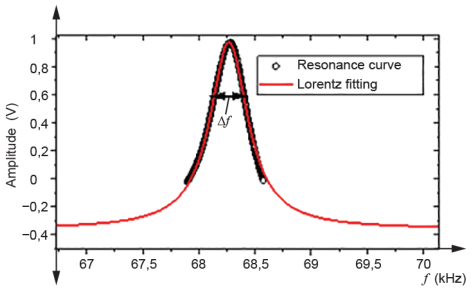	optional
4	(repeated) measurements of the raw data distribution of a reference sample with well-adjusted measurement height z	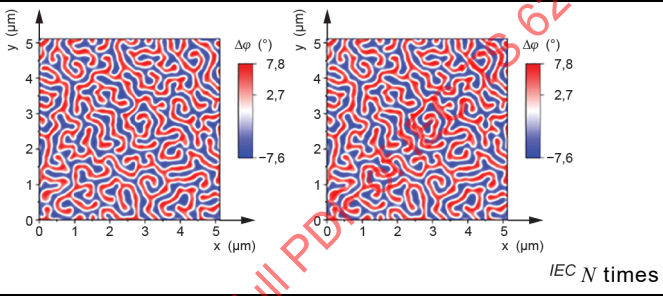	required
5	(repeated) measurements of the raw data distribution of the sample under test	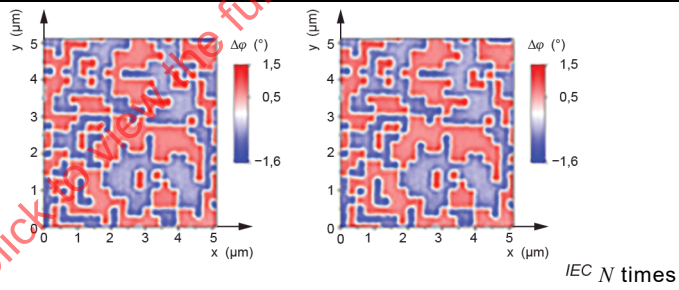	required
6	(repeated) measurements of the raw data distribution of the reference sample with identical parameters	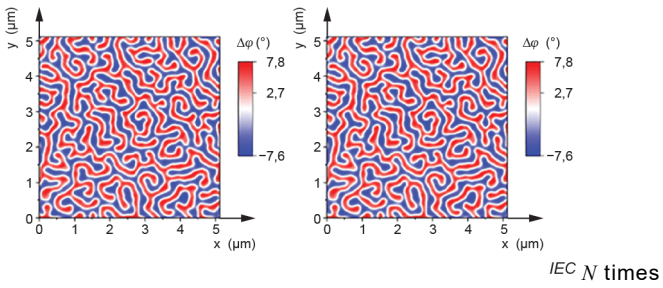	required
7	measurement of the cantilever quality factor Q using the manufacturer's software	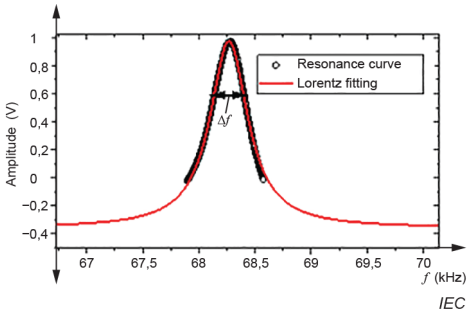	required
8a	data pre-processing, windowing, partial Fourier transformation		required

Step	Action	Illustration	Status
8b	selection of a deconvolution approach	"Default" or user defined. User defined deconvolution approach shall be documented.	required
8c	calculation of the F^{ICF} from steps 4) and 6) using the regularized deconvolution approach from step 8b) Details in 4.4.7.	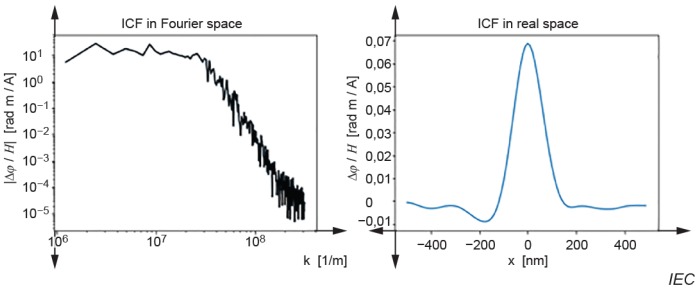	required
9	correction of the F^{ICF} for changed parameters as discussed under 4.4.6.		required
10	calculation of the quantitative magnetic field distribution of the sample under test from its raw data distribution by a regularized deconvolution with the corrected F^{ICF}.	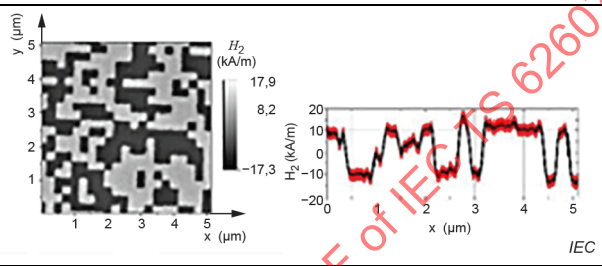	required

5.4 Measurement reliability

5.4.1 Artefacts in MFM measurements

Since MFM exploits the interaction between the magnetic tip and the magnetic sample, some artefacts resulting from the magnetic interaction are possible. They need to be ruled out to ensure that a tip calibration process can be successfully performed. Some typical artefacts are illustrated in the following for the example of a band domain sample.

5.4.2 Artefacts resulting from strong stray field samples

For low tip coercivity fields (e.g. approximately 30 mT for typical MFM tips), high sample stray fields and low measurement heights, repeated switching events of the tip magnetization can occur. Typical images for this type of artefact are shown in Figure 10.

In Figure 10 (left side), the sign of the phase shift does not switch between alternating band domains but within a domain (blue areas within red bands, e.g. as indicated by the black arrow). This can happen if the magnetization orientation of the tip is opposite to that of the sample in the red regions. When the tip reaches these areas, the magnetization of the tip is partially switched. When the tip moves to the blue regions, the reversed part of the tip switches back.

Another type of influence can be seen in Figure 10 (right side): several lines seem to be shifted compared to the "true" domain structure.

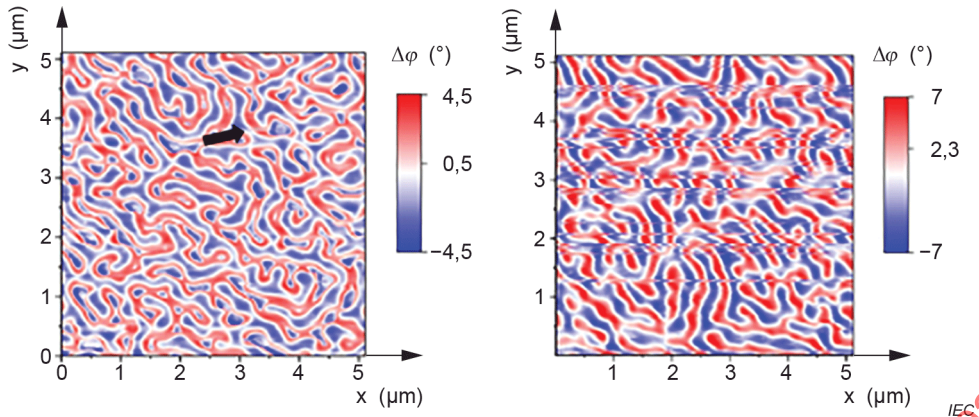

Figure 10 – Artefacts that occur if the tip magnetization is switched by the stray field of the sample

5.4.3 Artefacts when measuring samples with low coercivity

When the stray field of the tip is high and the coercivity of the sample is low, the tip can switch the magnetization of the sample. Figure 11 shows two MFM images (a) and (b) taken from consecutive MFM measurements. The original domain structure was a homogeneous magnetization with the magnetization orientation opposite to the tip magnetization (red colour), as indicated by the lower part in Figure 11(a). However, during the MFM measurement, the homogeneous magnetization was gradually switched by the stray field of the tip into a multi-domain structure.

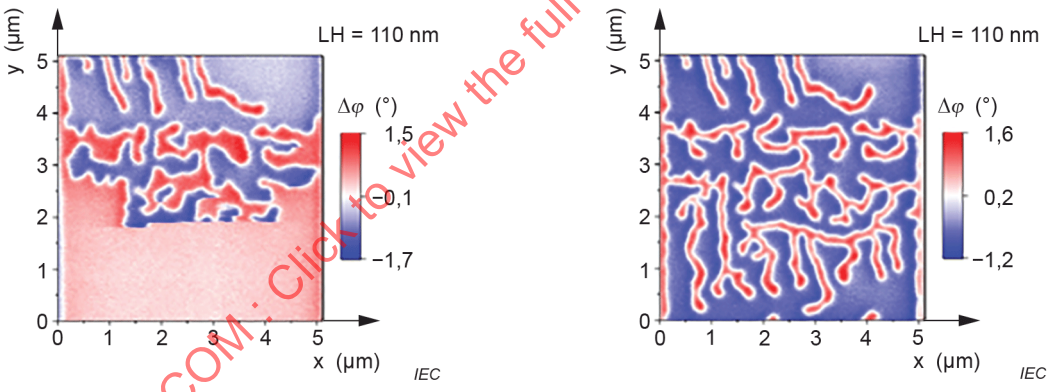

Figure 11 – Artefacts if the sample domain orientation is switched by a strong tip stray field

5.4.4 Distortion of the domain structure

Figure 12 shows a typical distortion of the domain structure of the reference sample. Band domains with one orientation appear much broader than the domains with the opposite orientation. A measurement distorted in such manner can not be used for the tip calibration.

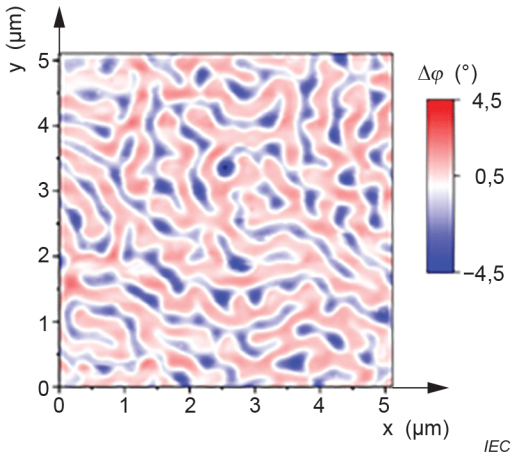

Figure 12 – Typical distortion of an MFM image: different domain widths

5.4.5 Contingency strategy

The described artefacts are examples for effects of the interactions between sample stray field and tip magnetization, or tip stray field and sample magnetization. High stray fields lead to switching events or distortions of the magnetization. Measurements that show artefacts shall not be used for calibration. The detrimental impact of the tip sample interaction can be reduced in the following ways:

- increasing the tip–sample distance (if either tip or sample is distorted). However, in the usual two-pass mode, this only helps if the interaction during the topography scan is reversible;
- using tips with a lower magnetic moment (if the sample magnetization is distorted);
- using tips with higher coercivity (if the tip is switched by the sample).

To decide whether the MFM image correctly represents the domain structure of the sample under test requires prior knowledge of the magnetic properties of the test sample. The user shall check the plausibility of the measured image.

5.4.6 Strategies to improve the quality of the measurements

- high signal-to-noise ratio (slow scan rate, repeated measurements);
- high Q;
- high field amplitude of the reference sample (but low enough not to switch the tip);
- low positioning uncertainty;
- low measurement heights (but high enough to avoid interactions);
- stable temperature.

5.5 Uncertainty evaluation

5.5.1 General

When performing a calibrated field measurement of a sample under test, the uncertainties of the different calibration steps enter into the uncertainty budget and shall be recorded for a quantitative analysis. The relevant contributions of the individual steps are summarized in 5.5.2 to 5.5.4.

5.5.2 Reference sample

The uncertainty of the magnetic field distribution, including the spatial coordinates (x,y), and of the magnetic field amplitudes.

If a band domain sample is used:

- the uncertainties of the sample parameters saturation magnetization M_S, thickness of the reference sample d, domain wall transition width δ_{DW};
- uncertainties related to the measurement: measurement height z, tip oscillation amplitude A_{osc}, canting angles θ and φ;
- uncertainties related to positioning inaccuracies (x,y);
- uncertainties related to the discrimination process.

NOTE It is possible that the band domain sample does not strictly follow the domain theory underlying the reference sample calculation, i.e. the assumptions of a perfect perpendicular magnetization and of Bloch-wall like transition cannot be fully met. The deviation is considered neglectable in the context of MFM under ambient conditions and is therefore not taken into account but can become relevant under measurement conditions where a very high resolution is achieved.

5.5.3 ICF determination

The uncertainty evaluation of the F^{ICF} considers type A and type B components.

Type A uncertainty is induced by noise in the measured reference sample raw data distributions (here: phase shift) and can be estimated by averaging F^{ICF} data from independent measurements on the reference sample.

Type B uncertainty consists of:

- uncertainties of key control parameters: MFM phase signal distribution $\Delta\varphi^{ref}$, pixel size ΔA, tip quality factor Q, measurement height z;
- the uncertainty of the magnetic field distribution of the reference sample;
- the uncertainty of the regularized deconvolution process.

5.5.4 Calibrated field measurement

The uncertainty evaluation of the F^{ICF} considers type A and type B components.

Type A uncertainty is induced by noise in the measured SUT raw data distribution (here: phase shift data) and can be estimated by averaging stray field data from independent calibrated measurements of the SUT.

Type B uncertainty consists of:

- uncertainties of key control parameters: phase signal of the MFM raw data distribution $\Delta\varphi$, pixel size ΔA, tip quality factor Q, measurement height z;
- the uncertainty of the F^{ICF};
- the uncertainty of the regularized deconvolution process.

Key control characteristics that are not changed between F^{ICF} determinations and calibrated measurements cancel out in the Type B uncertainty and only affect the Type A uncertainty.

Table 6 – Uncertainty evaluation key control characteristics

Key control characteristic	Identifier	Typical value	Relevance
Uncertainty contributions for stray field calculation of band domain samples			
saturation magnetic moment per unit area m_s	um_s	5 %	high
thickness of the reference sample d	ud	5 %	high
domain transition type and width δ_{DW}	$u\delta_{DW}$	20 %	low
measurement height z^{ref}	uz^{ref}	5 %	high
canting angles θ and φ	$u\theta$ and $u\varphi$	1 %, 1 %	low
Positioning inaccuracies (x,y)	ux, uy		strongly setup dependent
Uncertainty contributions for F^{ICF} determination			
uncertainty of reference stray field distribution H_z^{ref}	uH_z^{ref}	5 %	high
reference sample raw data distribution $\Delta\varphi^{ref}$	$u\Delta\varphi^{ref}$	2 %	high
regularization parameter α^{ref}	$u\alpha^{ref}$		low
Uncertainty contributions for calibrated stray field measurement			
uncertainty of F^{ICF}	uF^{ICF}	10 %	
phase signal of the MFM image $\Delta\varphi^{SUT}$	$u\Delta\varphi^{SUT}$	2 %	high
measurement height z^{ref}	uz^{ref}	5 %	high
tip oscillation amplitude A_{osc}^{ref}	uA_{osc}^{ref}	1 %	low
pixel size ΔA^{ref}	$u\Delta A^{ref}$	1 %	strongly setup dependent
tip quality factor Q^{ref}.	uQ^{ref}.	4 %	high
measurement height z^{SUT}	uz^{SUT}	5 %	high
tip oscillation amplitude A_{osc}^{SUT}	uA_{osc}^{SUT}	1 %	low
pixel size ΔA^{SUT}	$u\Delta A^{SUT}$	1 %	strongly setup dependent
tip quality factor Q^{ref}.	uQ^{ref}.	4 %	high
regularization parameter α^{SUT}	$u\alpha^{SUT}$		high

NOTE Uncertainties of measurement parameters like the tip quality factor Q do not come into effect if the parameters are constant during reference and SUT measurement.

For uncertainty evaluations and propagation according to Table 6, refer to ISO/IEC Guide 98-3 [25] and Annex B.

6 Data analysis / interpretation of results

6.1 Software for data analysis

The quantitative data analysis can be performed by any software implementing the required and discussed steps. An MFM calibration and subsequent calibrated field measurement can, for example, be performed with the open source software Gwyddion[2] [27]: The process is described here for Gwyddion 2.55 (released 2019-11-04).

---

2 Gwyddion is free and open source software, covered by GNU General Public License (GNUGPL). This information is given for the convenience of users of this document and does not constitute an endorsement by IEC. Equivalent products may be used if they can be shown to lead to the same results.

Gwyddion allows to import data from most manufacturers of MFMs. After the data import, two-dimensional data matrices are obtained. Gwyddion allows the data pre-processing and performs the required data processing steps, from MFM calibration using a band domain sample up to deconvolution of the field above sample under test. The relevant MFM KCCs can be entered when required for the operations related to the calibration and calibrated measurement steps are applied.

a) Gwyddion divides the raw data distribution, i.e. the phase shift data, by a factor $f = Q/c \cdot 180/\pi \cdot \mu_0 \cdot \Delta x \cdot \Delta y$ to obtain a so-called "pixel area MFM force gradient" acting on the tip.

b) Gwyddion calculates the TTF, not the ICF.

c) For the calculation of the TTF, Gwyddion uses a pseudo-Wiener deconvolution; however the optimum α is not calculated by the default process (L-curve criterion) but by applying a so-called TTF-width-criterion [14], in which the width of the real space representation of the transfer function is minimized.

Table 7 and Table 8 explain how to apply Gwyddion and the MFM manufacturer's software to the different analysis steps for calibrated stray field measurements (Table 8) and for the analysis of the band domain reference sample (Table 7).

Table 7 – Software implementation of stray field calculation of band domain samples

Action	Software package	Software implementation
measurement of a reference sample	MFM manufacturer's software	Not applicable
data import and pre-processing	WSxM or Gwyddion	Load data (phase in degrees or radians) from manufacturer's format (majority of formats) or as raw data (custom built microscopes). Data process → Correct Data – various scan line defects correction functions (e.g. scars, align rows)
level data	Gwyddion	Data Process → Level → Zero Mean Value
discrimination	Gwyddion	Data Process → Grains → Mark by Threshold → Threshold by Height: 50 %
calculation of the reference sample magnetic field distribution	Gwyddion	Data Process → SPM Modes → Magnetic → Perpendicular Media Field, then set a) output plane height b) film thickness c) magnetic charge d) cantilever angle e) include domain walls. If ticked: set f) exchange constant g) uniaxial anisotropy h) output type: Hz

Table 8 – Software-based realization of calibrated measurement

Action	Software package	Software implementation
characterizing cantilever quality factor Q	MFM manufacturer's software	Not applicable
measurement of a reference sample	MFM manufacturer's software	Not applicable
measurement of the raw data distribution (here: phase shift data) of the sample under test.	MFM manufacturer's software	Not applicable

Action	Software package	Software implementation
data import and pre-processing	WSxM [28] or Gwyddion [27]	Load data (phase in degrees or radians) from manufacturer's format (majority of formats) or as raw data (custom built microscopes). Data process → Correct Data – various scan line defects correction functions (e.g. scars, align rows).
level data	Gwyddion	Data Process → Level → Zero Mean Value
rescaling of phase data to force gradient	Gwyddion	Data Process → SPM modes → Magnetic → Recalculate to force gradient (inputting the probe's spring constant and Q factor) Selected "Pixel area MFM force gradient" as "Result type".
calculation of stray field distribution from reference data	Gwyddion	See steps Table 8
calculation of TTF from reference sample measurement by regularized deconvolution	Gwyddion	Data Process → Statistics → Transfer Function Guess – choose the ideal response (from the previous step) and calculation algorithm, see [14] for more details. Data Process → Distortion → Radial smoothing – use this to radially average the TTF if needed. Data Process → Multidata → Arithmetics – use this to merge multiple TTF results if needed.
quantitative magnetic field distribution by regularized deconvolution of the MFM data (SUT) with the corrected TTF	Gwyddion	Select rescaled MFM data from SUT, Data Process → Multidata → Deconvolve – select calculated TTF as kernel, update L curve. If the pixel size of the calculated TTF is different, resample TTF to the same pixel size prior to it.

7 Results to be reported

7.1 General

The results of the measurements shall be documented in a measurement report, including the date and time of the measurements as well as the name and signature of the person responsible for the report.

7.2 Product / sample identification

The report shall contain all information to identify the test sample and trace back the history of the sample:

- General procurement information, according to the blank detail specification <IEC 62565-X-Y>
- General material description according to the blank detail specification <IEC 62565-X-Y>, including a technical drawing:
  - top view, indicating the inspected area and location of the measurement positions;
  - cross section, showing the layer structure.

7.3 Test conditions

Example:

- temperature: 21,7 °C ± 0,1 °C
- relative humidity: (50 ± 4) %

7.4 Measurement set-up specific information

- scan rate (e.g. 5 µm/s);

- instrument (e.g. Bruker Dimension Icon®[3] system);
- tip producer and type name, tip properties (e.g. Nanosensors PPP-MFMR, hard magnetic coating on the tip side (coercivity of approximately 300 Oe, remanence magnetization of approximately 300 emu/cm, effective magnetic moment in the order of 10 emu to 13 emu);
- calibration status of equipment;
- typical measurement curve to visualize measurement accuracy;
- signal-to-noise ratio for the measurement curve.

7.5 Test results

- Sampling plan used:

  For example, coordinate system used in the measurement setup in absolute positions with a definition of the origin so that the measurement locations can be related to the technical drawing of the sample.

- Results of KCC measured in accordance with this document:

  For example, table of mean values and standard deviation of the KCC measured in accordance with this document at the positions defined by the sampling plan.

- Graphical visualization of KCC measured in accordance with this document:

  For example, in case of scanning methods: Colour maps for KCCs measured in accordance with this document. The colour map shall be scaled in absolute positions in respect of the origin of the coordinate system. The colour code should be calibrated in absolute values of the measured KCC.

8 Validity assessment

8.1 General aspects

In general, the transfer function resulting from the calibration only covers a limited section of the spatial Fourier spectrum and, without further knowledge, only holds at the specific grid points in Fourier space defined by the pixel size $\Delta x \times \Delta y$ and the image size $Sx \times Sy$. Furthermore, the deconvolution steps involved in the calibrated measurement process lead to an effective filtering in frequency space. This restricts the spatial frequency range covered by the calibration. The main aspects determining the effective useable set of frequencies where the calibration is valid are as follows.

1) The MFM tip has a finite coverage of spatial frequencies due to its magnetic geometry. Frequency components not contained in the tip's frequency spectrum are suppressed during the imaging process.
2) The reference sample has a finite coverage of spatial frequencies given by its magnetization pattern.
3) The accessible frequency spectrum of the reference sample measurement is additionally limited due to the broadening of stray fields at the measurement height z.
4) The accessible frequency spectrum of the reference sample measurement is further limited to low and high values by the finite and discrete nature of the measurement process, namely by the image size and by the pixel size. The discrete nature of the imaging process that results in $Nx \times Ny$ equidistant pixels leads to discrete grid points in Fourier space.
5) The signal-to-noise ratio of the reference and SUT measurement data in combination with the inverse filtering process lead to a further suppression of frequency components with small amplitudes comparable to or below the noise level.

[3] Dimension Icon® is the trademark of a product supplied by Bruker Corporation. This information is given for the convenience of users of this document and does not constitute an endorsement by IEC. Equivalent products may be used if they can be shown to lead to the same results.

The imaging process related restrictions, as listed under 4), are unavoidable; however, they do not, apart from edge effects, impact the quantitative field calculation of a SUT if the reference image and the SUT image are taken with equal discretization parameters, i.e. same image size and pixel size.

To minimize the impact of the other aspects, an optimum calibration of the setup requires a high overlap of the spatial frequency spectra of the MFM tip, the reference sample and the SUT. Frequencies that are not covered by either the tip or the reference sample are suppressed during the calibration and during the subsequent calibrated measurement. Most notably, the Fourier spectrum of the tip's stray field gradient distribution typically shows a rapid decay towards high frequencies. Depending on the noise level, this leads to an upper cut-off frequency (lower limit wavelength) for the F^{ICF}. Typical cut-off-wavelengths $k^{\text{cut-off}}$ for commercial MFMs operated at room temperature amount to some 10 nm.

Therefore, the user needs to be aware that the calibrated stray field distribution of the SUT a priori only shows a real space representation of a calibrated frequency space distribution, with a limited value range in frequency space and therefore the measured stray field distribution can significantly deviate from the physical data of the SUT.

Users are strongly advised to check the overlap and thus the validity range of their calibrated measurement data. Additionally, DC field offsets are always suppressed since they are not detected by the measurement technique described in this document. In addition to the physical properties of the involved samples and the tip, the numerical analysis process (the inverse filtering) in combination with the measurement signal-to-noise ratio also can have significant impact on the net effective filtering characteristics of the calibrated measurement process.

8.2 Requirements

Based on the above considerations, the following practice requirements shall be followed to achieve an accurate representation of the SUT stray field distribution and to assess the validity of the results.

- Reference and SUT measurement shall have equal image size and pixel numbers.
- The spatial Fourier spectra of the reference sample and the SUT shall overlap significantly. The overlap shall be controlled.
- The impact of the inverse filtering shall be carefully assessed.
- If the filtering in either the calibration or the calibrated measurement process is found to suppress relevant SUT features, this shall be stated together with the calibrated field data.

8.3 Example

8.3.1 Determination of the Instrument Calibration Function F^{ICF}

Uncertainties for F^{ICF} values at $\boldsymbol{k}$-vectors with finite but low signal amplitude are induced by the signal-to-noise ratio of the raw measurement data that leads to a limitation of the effective spectral coverage. This is demonstrated in Figure 13. Figure 13 a) shows the Fourier spectrum of the reference sample phase shift data $\Delta\varphi^{\mathrm{ref}}$ together with the estimated magnetic field data H_z^{ref}. These data sets are used in the calibration process to calculate the F^{ICF} using a pseudo-Wiener filter, as discussed in Formula (9):

$$F_{\alpha}^{\mathrm{ICF,ref}}\left(\boldsymbol{k},z\right)=\Delta\varphi^{\mathrm{ref}}\left(\boldsymbol{k},z\right)\frac{H_z^{\mathrm{ref*}}\left(\boldsymbol{k},z\right)}{\left|H_z^{\mathrm{ref}}\left(\boldsymbol{k},z\right)\right|^2+\alpha}$$

The optimum regularization parameter α depends on the signal-to-noise ratio of the $\Delta\varphi^{\mathrm{ref}}$ data. The α-dependent filtering leads to a suppression of frequency components with amplitudes lower than or comparable to the noise level. To obtain a good first estimate of the impact of the

pseudo-Wiener filter on the calculated F^{ICF}, one can compare it to a direct deconvolution as is realized by the division $\Delta\varphi^{\mathrm{ref}}(\boldsymbol{k},z)$ / $H_z^{\mathrm{ref}}(\boldsymbol{k},z)$. We define a filter ratio R^{F} as

$$R^{\mathrm{F}} = \Delta\varphi^{\mathrm{ref}}(\boldsymbol{k},z)\frac{H_z^{\mathrm{ref}*}(\boldsymbol{k},z)}{\left|H_z^{\mathrm{ref}}(\boldsymbol{k},z)\right|^2+\alpha} \Bigg/ \frac{\Delta\varphi^{\mathrm{ref}}(\boldsymbol{k},z)}{H_z^{\mathrm{ref}}(\boldsymbol{k},z)} = H_z^{\mathrm{ref}}(\boldsymbol{k},z)\frac{H_z^{\mathrm{ref}*}(\boldsymbol{k},z)}{\left|H_z^{\mathrm{ref}}(\boldsymbol{k},z)\right|^2+\alpha} = \frac{\left|H_z^{\mathrm{ref}}(\boldsymbol{k},z)\right|^2}{\left|H_z^{\mathrm{ref}}(\boldsymbol{k},z)\right|^2+\alpha}$$

The R^{F} depends on α and should be plotted for the α that results from the filter optimization process (in this example: L-curve criterion).

In Figure 13 b) R^{F} is plotted as a function of the wave vector. For low filter ratios the resulting F^{ICF} components are significantly impacted and cannot be regarded as reliable. Thus, the calibrated measurement does not give reliable results at these spatial frequencies. F^{ICF} amplitudes resulting from frequencies showing a filter ratio close to 1 are as a rule reliable and lead to a low error.

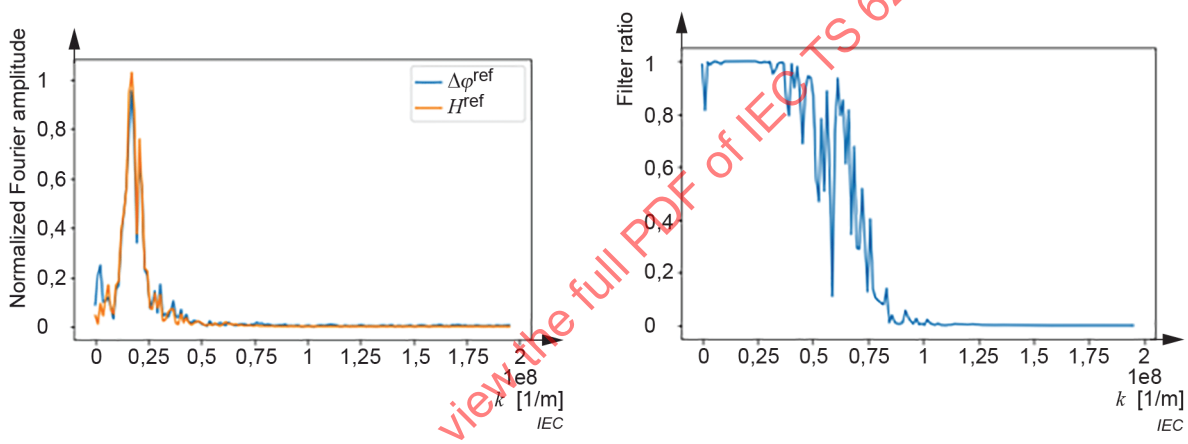

a) at tip apex H^{ref} **b) filter ratio R^{F} as a function of the wave vector**

NOTE The filter ratio is shown for an optimum α as resulting from the L-curve method.

Figure 13 – Normalized Fourier amplitudes of the measured reference sample signal $\Delta\varphi^{\mathrm{ref}}$ and the reference sample magnetic field

Tracing the filter optimization process gives further insight into the useable set of frequencies. Figure 14 shows the F^{ICF} in Fourier space as it results from different regularization parameters α that are lower than or equal to the optimum α, as it results from the L-curve criterion. Increasing α towards the optimum value leads to an increasing suppression of high frequency components of the calculated F^{ICF}. These high frequency F^{ICF} values that strongly depend on α are not genuine frequencies of the magnetic samples but are evoked by noise in the measured phase shift signal. Unless these contributions are filtered out, the real space representation of the F^{ICF} is dominated by noise, Figure 14 b). The dotted grey line in Figure 14 a) marks the estimated upper limit for valid k-values, $k^{\mathrm{cut\text{-}off}}$.

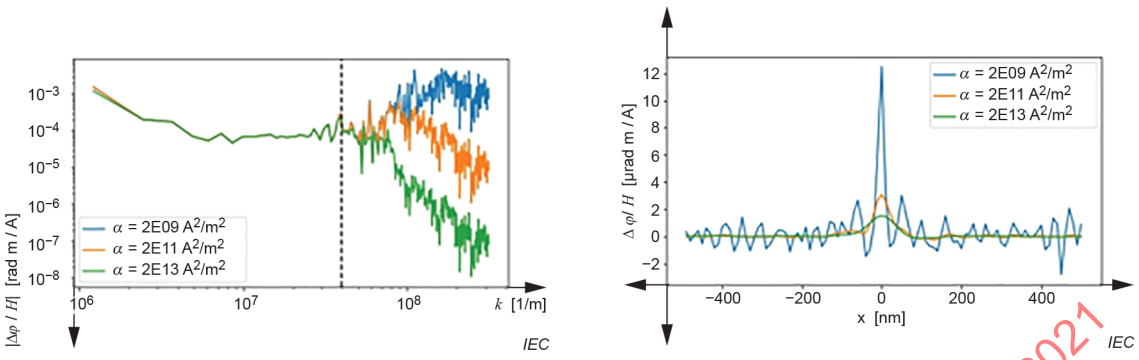

a) Fourier space b) Real space

NOTE The green line shows the ICF for an optimized α as it results from the L-curve criterion. ICF frequency components for high k-values are noise dominated and need to be suppressed by the inverse filtering.

Figure 14 – Typical transfer functions in Fourier and real space for different values of the regularization parameter α

The filter ratio plot as well as the α dependency of the F^{ICF} lead to a $k^{\text{cut-off}}$ of about 4 × 10^7 m^{-1}.

8.3.2 Calibrated measurement

Similar considerations apply to the calibrated measurement process.

Figure 15 shows MFM phase shift images of a) the reference sample and b) a SUT, together with c) a line plot of the Fourier spectra of the phase shift data of the reference sample and the SUT (in k_x-direction). Such plots can be used to assess the overlap in the relevant frequency range. In the example, inspection of the relevant graphs shows that the relevant frequency components of the SUT (high amplitudes) are covered by the calibration process. However, for frequencies with k-vectors with amounts larger than 4 × 10^7 m^{-1} one should consider the possibility of significant uncertainties of the resulting F^{ICF} values.

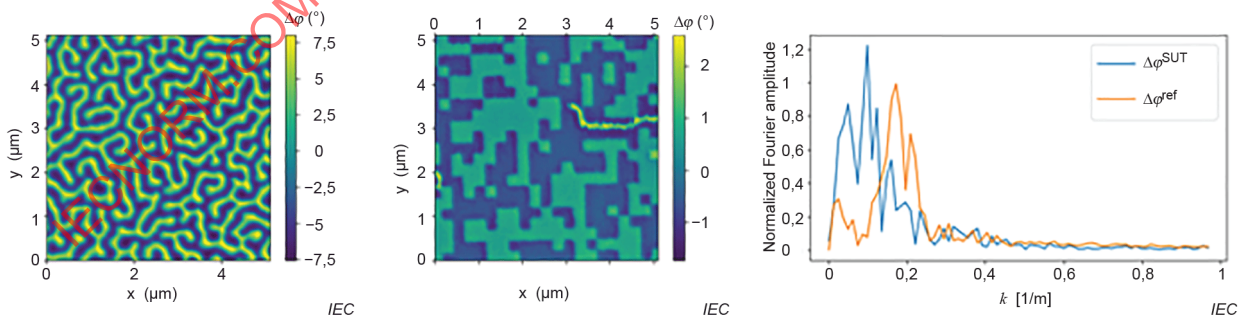

a) Reference sample MFM signal $\Delta\varphi^{\mathrm{ref}}$ b) SUT MFM signal $\Delta\varphi^{\mathrm{SUT}}$ in real space c) Fourier spectra of signal $\Delta\varphi^{\mathrm{ref}}$ and signal $\Delta\varphi^{\mathrm{SUT}}$

Figure 15 – Comparison of the reference sample signal $\Delta\varphi^{\mathrm{ref}}$ and the SUT signal $\Delta\varphi^{\mathrm{SUT}}$

The uncertainty of the evaluation as discussed in Annex B correctly assesses the impact of the measurement and parameter uncertainties on the resulting F^{ICF}, i.e. robustness of the processing of the F^{ICF}. However, this uncertainty is not identical with the intrinsic uncertainty of the F^{ICF}, which might be higher. This latter uncertainty is a consequence of the filtering and

of systematic uncertainties arising from spatial frequencies not covered in the reference sample or the tip.

Therefore, the calibration, together with its uncertainty as discussed in Annex B, holds for the common discrete spatial frequency support set of the reference sample and the tip. However, predictions on F^{ICF} values for other spatial frequencies interpolating or extrapolating from the discrete set data points covered by the calibration are not per se possible (unless the user has further knowledge on the tip properties). As a consequence, the calibrated field measurement together with its uncertainty is correct if and only if it is understood with regard to this exact set of frequencies.

Annex A
(informative)

Algorithm

A.1 Mathematical basics

A.1.1 Continuous Fourier transform versus discrete Fourier Transform

The continuous Fourier transform $F(k_x,k_y)$ of a 2D-function $f(x,y)$ is defined as

$$F\left(k_x,k_y\right)=\iint f\left(x,y\right)e^{-ik_x x-ik_y y}\mathrm{d}x\mathrm{d}y\ .$$

However, MFM data typically are taken at discrete sampling points in the form of a pixel image $f^{\mathrm{D}}(x,y)$ with a pixel number $Nx \times Ny$ over an image size $Sx \times Sy$. The resulting pixel size $\Delta x \times \Delta y$ can be calculated from $\Delta x = Sx/Nx$ and $\Delta y = Sy/Ny$. Note: Different MFM systems can have different definitions of Δx, Δy, Sx, Sy, Nx and Ny. The discrete Fourier transform $F(u,v)_{\mathrm{DFFT}}$ on $f^{\mathrm{D}}(m,n)$ is defined as

$$F\left(k,l\right)_{\mathrm{DFFT}}=\sum_{m=0}^{Nx-1}\sum_{n=0}^{Ny-1}f^{\mathrm{D}}\left(m,n\right)e^{-2\pi i\left(\frac{mk}{Nx}+\frac{nl}{Ny}\right)}\ \text{with}\ k\in\{0,1,\ldots Nx-1\}\ ,l\in\{0,1,\ldots Ny-1\} \tag{A.1}$$

The corresponding wave vectors k_x and k_y that are used further below for field calculations can be calculated from the pixel dimensions in in k-space dk_x and dk_y. mod is the modulo operator.

$$dk_x=\frac{2\pi}{Nx\,\Delta x}=\frac{2\pi}{Sx}\qquad k_x(u)=\left(\left(u+\frac{Nx}{2}\right)\mathrm{mod}\ Nx-\frac{Nx}{2}\right)\cdot dk_x$$

$$dk_y=\frac{2\pi}{Ny\,\Delta y}=\frac{2\pi}{Sy}\qquad k_y\left(u\right)=\left(\left(u+\frac{Ny}{2}\right)\mathrm{mod}\ Ny-\frac{Ny}{2}\right)\cdot dk_y$$

A.1.2 Partial (two-dimensional) Fourier space

The partial 2D Fourier transform $F(\boldsymbol{k},z)$ of a function $f(\boldsymbol{r},z)$ is defined as

$$F\left(\boldsymbol{k},z\right)=\iint f\left(\boldsymbol{r},z\right)e^{-ik_x x-ik_y y}\,\mathrm{d}x\,\mathrm{d}y \tag{A.2}$$

With $\boldsymbol{k} = (k_x,k_y)$ and $\boldsymbol{r} = (x,y)$.

A.1.3 Cross correlation theorem

A cross correlation $f * g$ between two functions f and g is defined as

$$f\left(t\right)*g\left(t\right)=\int f\left(\tau\right)g\left(t+\tau\right)\mathrm{d}\tau$$

The Fourier transform of a cross-correlation product is

$$\mathcal{F}\left(f*g\right)=F^{*}\cdot G \tag{A.3}$$

where the asterisk * denotes the complex conjugate and capital letters denote the Fourier transform.

A.2 Magnetic fields in partial Fourier space

A.2.1 Differentiation in partial Fourier space

In a region in which the magnetic field is rotation free, the partial Fourier space Nabla operator ∇ becomes

$$\nabla(\boldsymbol{k}) = \nabla_k = \left(ik_x, ik_y, -k\right) \tag{A.4}$$

with $k = \sqrt{k_x^2 + k_y^2}$.

A.2.2 Magnetic fields in partial Fourier space

In 2D partial Fourier space and in a region where the magnetic field is rotation free, all components of the field vector $\boldsymbol{H}$ can be calculated from its z-component

$$\boldsymbol{H}(\boldsymbol{k}, z) = -\frac{1}{k}\nabla_k H_z(k, z) \tag{A.5}$$

And thus

$$H_z(\boldsymbol{k}, z) = H_z(\boldsymbol{k}, z')e^{-ik(z-z')} \tag{A.6}$$

A.3 Signal generation in magnetic force microscopy

A.3.1 General

The following discussion closely follows the description given in [19].

The force acting on the MFM tip in the stray field of the sample can be written as

$$\boldsymbol{F}(\boldsymbol{r}, z) = \mu_0 \int_{r'z'} \nabla M^{\text{tip}}(r', z')\, \boldsymbol{H}^{\text{sample}}(\boldsymbol{r} + \boldsymbol{r}', z + z')\, \mathrm{d}\boldsymbol{r}'\mathrm{d}z'$$

Here, $\boldsymbol{r} = (x, y)$ and $\boldsymbol{r}' = (x', y')$. Formula (A.2) represents a 3D cross correlation integral. When applying the cross-correlation theorem only to the x-y-integral, only the x and y coordinates are transformed to the partial Fourier space

$$
\begin{aligned}
\boldsymbol{F}(\boldsymbol{k},z) &= \mu_0 \int_z \nabla_{\boldsymbol{k}}^{*} \cdot \boldsymbol{M}^{\text{tip}^*}(\boldsymbol{k},z')\boldsymbol{H}^{\text{sample}}(\boldsymbol{k},z+z')\,\mathrm{d}z' \\
&= \mu_0 \int_z \begin{pmatrix} -ik_x \\ -ik_x \\ -k \end{pmatrix} \boldsymbol{M}^{\text{tip}^*}(\boldsymbol{k},z')\boldsymbol{H}^{\text{sample}}(\boldsymbol{k},z)e^{-ikz'}\,\mathrm{d}z' \\
&= \mu_0 \boldsymbol{H}^{\text{sample}}(\boldsymbol{k},z) \int_z \begin{pmatrix} -ik_x \\ -ik_x \\ -k \end{pmatrix} \boldsymbol{M}^{\text{tip}^*}(\boldsymbol{k},z')e^{-ikz'}\,\mathrm{d}z' \\
&\equiv \mu_0 \boldsymbol{H}^{\text{sample}}(\boldsymbol{k},z)\sigma^{\text{tip}^*}(\boldsymbol{k})
\end{aligned}
\tag{A.7}
$$

$\sigma^{\text{tip}^*}(\boldsymbol{k})$ is the equivalent magnetic surface of the tip projected onto a plane through the tip apex:

$$
\sigma^{\text{tip}^*}(\boldsymbol{k}) = \int_z \begin{pmatrix} -ik_x \\ -ik_x \\ -k \end{pmatrix} M^{\text{tip}^*}(\boldsymbol{k},z')e^{-ikz'}\,\mathrm{d}z'
$$

The magnetic imaging properties of the tip are fully covered by σ^{tip}.

The magnetic field emerging from the tip, H_z, and its derivative $\frac{\partial H_z}{\partial z}$ can both be calculated from $\sigma^{\text{tip}}(\boldsymbol{k})$:

$$
\frac{\partial H_z^{\text{tip}}(\boldsymbol{k},z)}{\partial z} = -k\, H_z^{\text{tip}}(\boldsymbol{k},z) = \frac{k}{2}\sigma_{\text{tip}}(k)
\tag{A.8}
$$

In Formula (A.7) the magnetic field $H^{\text{sample}}(\boldsymbol{k},z)$ can be replaced with Formula (A.5):

$$
\boldsymbol{F}(\boldsymbol{k},z) = -\mu_0\, \sigma^{\text{tip}^*}(k)\frac{1}{k}\nabla_k H_z(k,z)
\tag{A.9}
$$

A.3.2 MFM phase shift signal

In typical magnetic force microscopes, the long axis of the tip is canted compared to the sample surface normal by an angle θ and the cantilever can be rotated away from the x-axis in the sample plane by an angle φ. The tip axis is described by the normalized vector

$$
\boldsymbol{n} = \left(\sin(\theta)\cos(\varphi),\, \sin(\theta)\sin(\varphi),\, \cos(\theta)\right)
\tag{A.10}
$$

The MFM signal in radian can be calculated from the gradient of the force acting on the tip in the direction of the oscillation of the tip (Q is the tip quality factor, C is the cantilever stiffness)

$$
\Delta\varphi(\boldsymbol{k},z) = \pm\frac{Q}{C}\cdot\boldsymbol{n}\nabla\boldsymbol{F}_{\boldsymbol{n}}
\tag{A.11}
$$

with $\boldsymbol{F}_{\boldsymbol{n}} = \boldsymbol{n}\boldsymbol{F}$ and $\boldsymbol{n}$ as described in Formula (A.10). Formula (A.11) can be evaluated for two limiting cases, namely "small" and "finite" oscillation amplitudes A_{osc} of the cantilever. The oscillation amplitude can be regarded as "small" if the change of $\boldsymbol{n}\nabla\boldsymbol{F}_{\boldsymbol{n}}$ along the trajectory of the oscillating tip is negligible. Otherwise, the phase shift can be calculated from an integration of Formula (A.11) over an oscillation cycle.

For the two limiting cases the following relations can be derived as demonstrated by [19]:

small amplitudes:
$$\Delta\varphi(\boldsymbol{k},z) = \mp\mu_0\,\sigma^{\text{tip*}}\,\frac{Q}{C_{\text{tip}}}\left(-\frac{1}{k}\boldsymbol{n}\nabla_{\boldsymbol{k}}\right)^2\cdot k\cdot H_z(\boldsymbol{k},z) \tag{A.12}$$

finite amplitudes:
$$\Delta\varphi(\boldsymbol{k},z) = \mp\mu_0\,\sigma^{\text{tip*}}\,\frac{Q}{C}\cdot\frac{2}{A_{\text{osc}}}\left(-\frac{1}{k}\boldsymbol{n}\nabla_{\boldsymbol{k}}\right)I_1\left(A_{\text{osc}}\,\boldsymbol{n}\nabla_{\boldsymbol{k}}\right)H_z(\boldsymbol{k},z) \tag{A.13}$$

$I_1(\chi)$ is the first order modified Bessel function of the first kind. The finite amplitude formula can be further evaluated using Formula (A.8):

$$\Delta\varphi(\boldsymbol{k},z) = \mp\frac{2\mu_0 Q}{C}\cdot F^{\text{LCF}}(\boldsymbol{k},\theta,\varphi,A_{\text{osc}})\cdot H_z^{\text{sample}}(\boldsymbol{k},z)\cdot\frac{\partial H_z^{\text{tip*}}(\boldsymbol{k},z)}{\partial z} \tag{A.14}$$

with the lever correction function $F^{\text{LCF}}(\boldsymbol{k},\theta,\varphi,A_{\text{osc}})$ defined as

$$F^{\text{LCF}}(\boldsymbol{k},\theta,\varphi,A_{\text{osc}}) = \left(-\frac{1}{k}\boldsymbol{n}\nabla_{\boldsymbol{k}}\right)^2\cdot\sum_{m=0}^{\infty}\frac{1}{m!(m+1)!}\left(\frac{\chi}{2}\right)^{2m}, \tag{A.15}$$

where $\chi = A_{\text{osc}}\,\boldsymbol{n}\nabla_{\boldsymbol{k}}$.

A.3.3 L-curve criterion for pseudo-Wiener filter-based deconvolution process

The L-curve criterion allows to find a unique regularization parameter α to be used in the pseudo-Wiener deconvolution approach:

$$G(\boldsymbol{k},z) = H(\boldsymbol{k},z)F(\boldsymbol{k},z)$$

$$F(\boldsymbol{k},z) = G(\boldsymbol{k},z)\frac{H^*(\boldsymbol{k},z)}{|H(\boldsymbol{k},z)|^2+\alpha}$$

The impact of the regularization parameter is illustrated in Figure A.1 for the example of a calculation of a TTF. As shown in the figures, with decreasing α the residual between initial data G and restored data $F_\alpha H$ as calculated from the F_α resulting from the deconvolution tends to zero. However, with decreasing α the F_α (here the TTF) deviates more and more from a physically reasonable profile and its 2-norm diverges due to noise amplification.